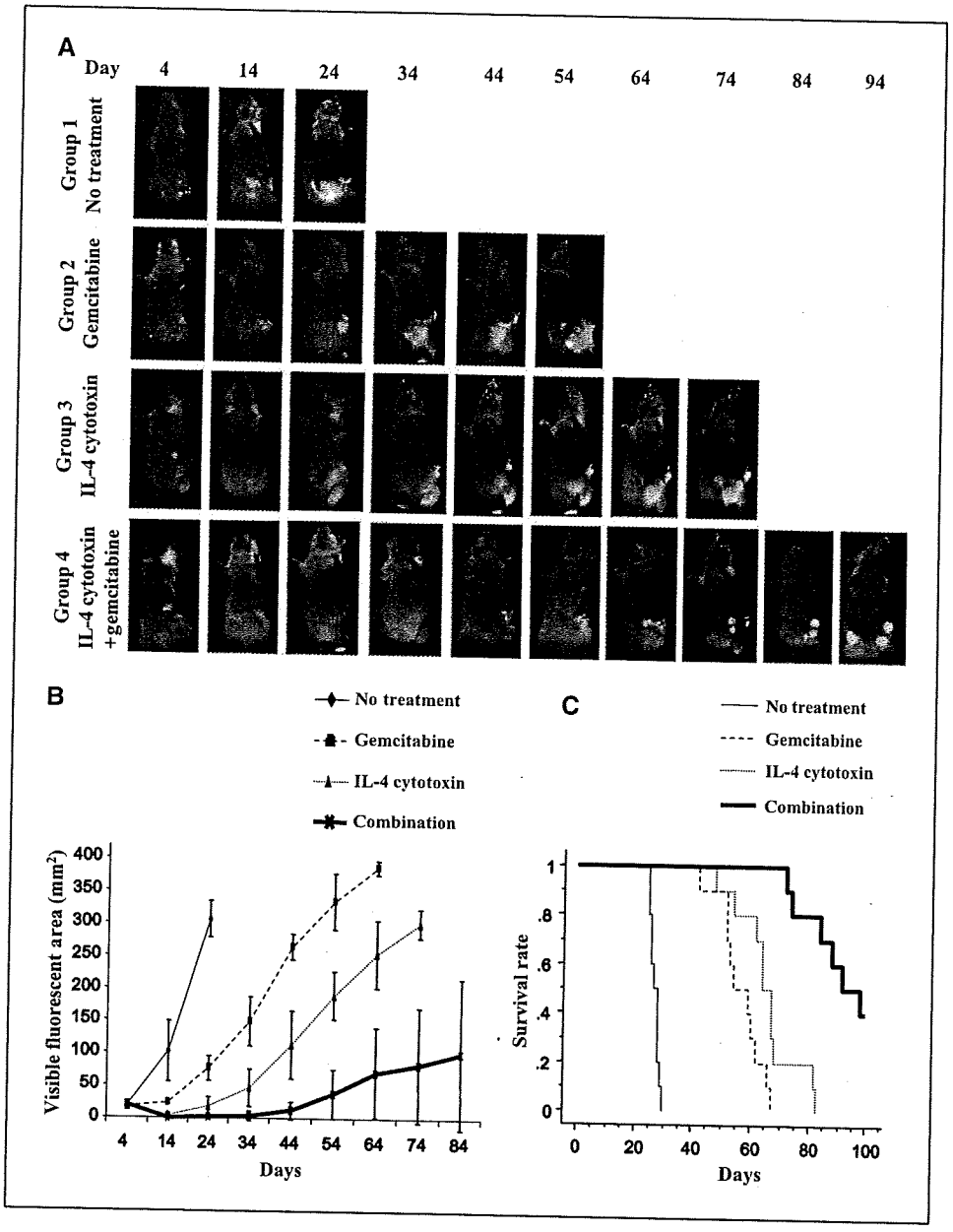

Figure 3. Sequential whole-body imaging, quantification of tumor volume, and real-time analysis of pancreatic tumor growth in an early tumor model. *A*, sequential *in vivo* imaging of tumor progression over time in early pancreatic cancer mice model. Selective tumor GFP fluorescence facilitated real-time visualization of tumor burden in the live animal. Panels depict a representative mouse from each of four groups. Treatment was initiated on day 5. Images are captured every 10 d beginning on day 4. Group 1 served as the negative control and did not receive any treatment. Group 2 received gemcitabine (150 mg/kg) by i.p. administration twice a week as long as the experiment lasted. Group 3 received IL-4 cytotoxin (100 μg/kg) by i.p. route twice a day for 5 d. Group 4 animals were treated with the combination of gemcitabine and IL-4 cytotoxin. *B*, quantification of primary and metastatic tumor GFP fluorescence enabled real-time determination and comparison of tumor load during the course of each treatment and, therefore, permitted real-time comparison of treatment efficacy between groups. *Points*, mean area of GFP fluorescence for live intact animals in each treatment group (n = 10 mice); *bars*, SE. *C*, Kaplan-Meier survival curves (n = 10 mice) of pancreatic cancer model after treatment with gemcitabine (150 mg/kg, twice a week after day 5), IL-4 cytotoxin (100 μg/kg, twice a day during days 5–9), and their combination.

was observed of IL-4 cytotoxin–treated mice (P = 0.0037) and the combination group (P < 0.0001). Prolonged survival time in the combination group was 216% compared with the nontreatment group.

Discussion

We show that 60% PDA samples express moderate- to high-density surface IL-4Rs, whereas normal pancreas express no or very low levels of IL-4R. IL-4 cytotoxin is highly cytotoxic to pancreatic cancer cell lines; however, it was not cytotoxic to HPDE cells, fibroblasts, and HUVEC, which express no or low levels of IL-4R. We also show that IL-4 cytotoxin synergizes with gemcitabine in mediating cytotoxic activity in pancreatic cancer cell lines *in vitro*, and in animal models of human pancreatic cancer *in vivo*. A significant prolonged survival effect of IL-4 cytotoxin and its combination with gemcitabine was shown in mice with early disease. Forty percent of mice that received combination therapy showed complete eradication of pancreatic tumors. In addition, this significant survival benefit was also confirmed in animals implanted with the clinical pancreatic cancer sample.

Gemcitabine (Gemzar) is a widely accepted first-line therapy for advanced pancreatic cancer, although the median survival time continues to be <6 months for these patients (2, 3). As most studies using single agent show low response rate and little effect on patient survival in advanced adenocarcinoma, several clinical trials using a combined approach of radiotherapy and/or molecular target therapy with gemcitabine have been initiated (33). *In vitro* studies have reported synergistic effect of gemcitabine with cisplatin, fluvastatin hydroxymethylglutaryl-CoA reductase inhibitor, CpG-oligodeoxynucleotides, EGFR, PDGF, and vascular endothelial growth factor inhibitor targeting drugs (6, 34–37). In

addition, immunotoxins were shown to exert synergistic effect with chemotherapeutic drugs, for example, doxorubicin plus anti-B4-blocked ricin, Ara-C plus granulocyte macrophage colony-stimulating factor fused to truncated diphtheria toxin (DT388-GM-CSF), and fludarabine with rituximab saporin-S6 conjugated protein (38–40). These studies support our observations of gemcitabine synergizing with IL-4 cytotoxin. Despite synergistic effect with gemcitabine, few combinations have shown clinical advantage (4–7). For example, although EGFR inhibitor showed synergistic antitumor effect in preclinical models, the survival benefits for patients with advanced pancreatic cancer seem very modest at best. It was later found that mutations in the *EGFR* gene, which correlate with clinical response, are found in <5% of pancreatic cancer patients (8, 41). Therefore, new effective therapies that do not depend on receptor mutation are needed. As our results show the survival benefit by IL-4 cytotoxin when combined with gemcitabine in both early and advanced pancreatic cancer models, it is possible that this novel approach will afford better tumor responses than previously observed.

The precise mechanism of synergistic effect of gemcitabine with IL-4 cytotoxin is not known. Gemcitabine is a synthetic pyrimidine antimetabolite structurally related to cytarabine (42). Gemcitabine inhibits DNA synthesis through inhibition of ribonucleotide reductase and depletion of deoxynucleotide pools. On the other hand, IL-4 cytotoxin inhibits protein synthesis after internalization into an endosome. In addition, we have previously shown that IL-4 cytotoxin can cause apoptotic cell death of cancer cells regardless of the cell cycle status (43). It is possible that gemcitabine enhances apoptotic cell death induced by IL-4 cytotoxin. Because apoptosis is a prominent mechanism of cancer cell death, the combination therapy of these drugs, which act through different mechanism, may be a beneficial treatment option for patients with PDA.

We studied two types of advanced pancreatic cancer models to show the antitumor activity of IL-4 cytotoxin and gemcitabine. In orthotopic model, the freshly resected clinical tumor was implanted to pancreas of SCID mice. It has been reported that this model recapitulates the natural history of the clinical disease,

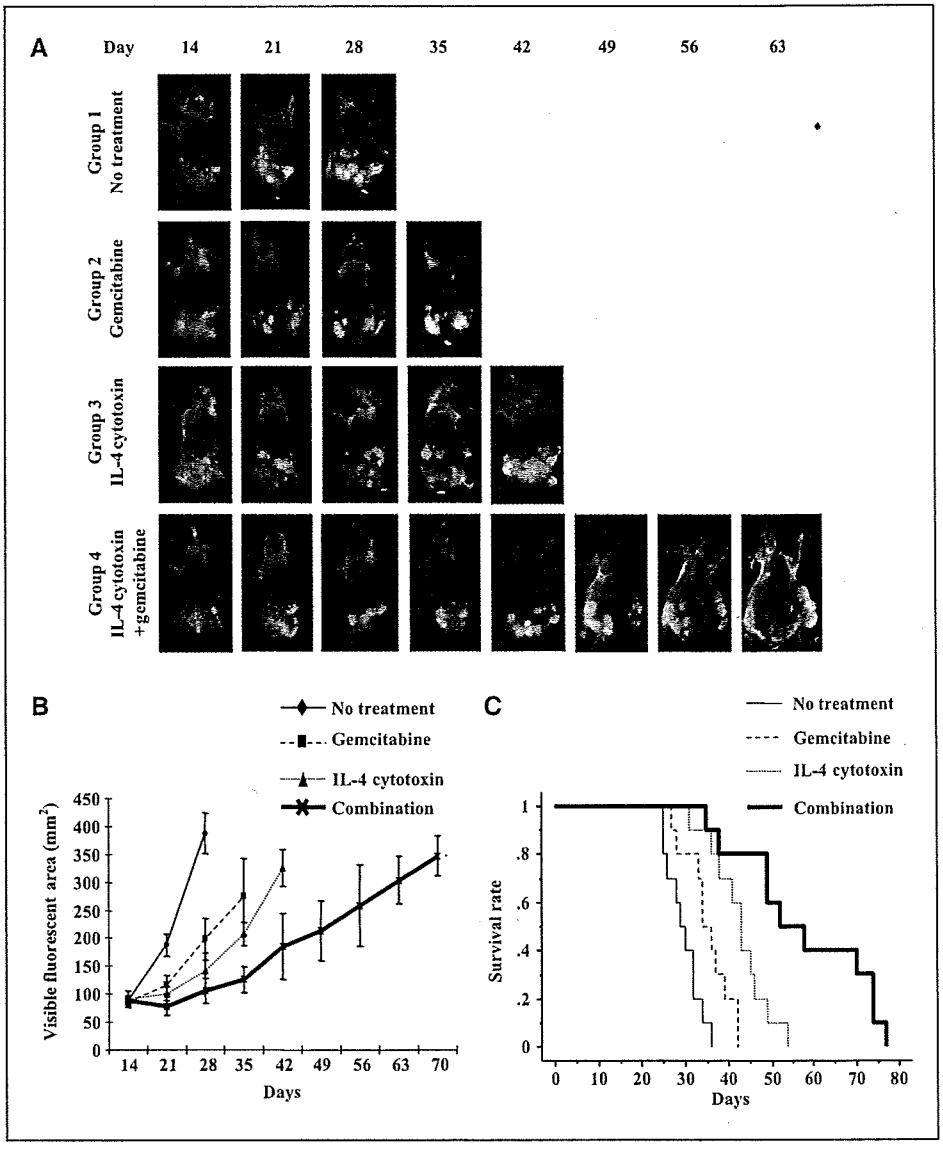

Figure 4. Sequential whole-body imaging, quantification of tumor volume, and real-time analysis of pancreatic tumor growth in an advanced tumor model. *A*, sequential *in vivo* imaging of tumor progression over time in advanced pancreatic cancer model. Selective tumor GFP fluorescence facilitated real-time visualization of tumor burden in live animals. Panels depict a representative mouse from each of four groups. Each group had 10 mice. Treatment was done after the confirmation of metastasis lesions on days 14. Images are captured every week after day 14. Group 1 served as the negative control and did not receive any treatment. Group 2 received gemcitabine (150 mg/kg) by i.p. administration twice a week as long as the experiment lasted. Group 3 received IL-4 cytotoxin (100 μg/kg) by i.p. route twice a day for 5 d. Group 4 animals were treated with the combination of gemcitabine and IL-4 cytotoxin. *B*, quantification of primary and metastatic tumor GFP fluorescence similar to Fig. 3*B*. *C*, Kaplan-Meier survival curves ($n = 10$ mice) with advanced PDA after treatment with gemcitabine (150 mg/kg, twice a week), IL-4 cytotoxin (100 μg/kg, twice a day during days 15–19), and their combination.

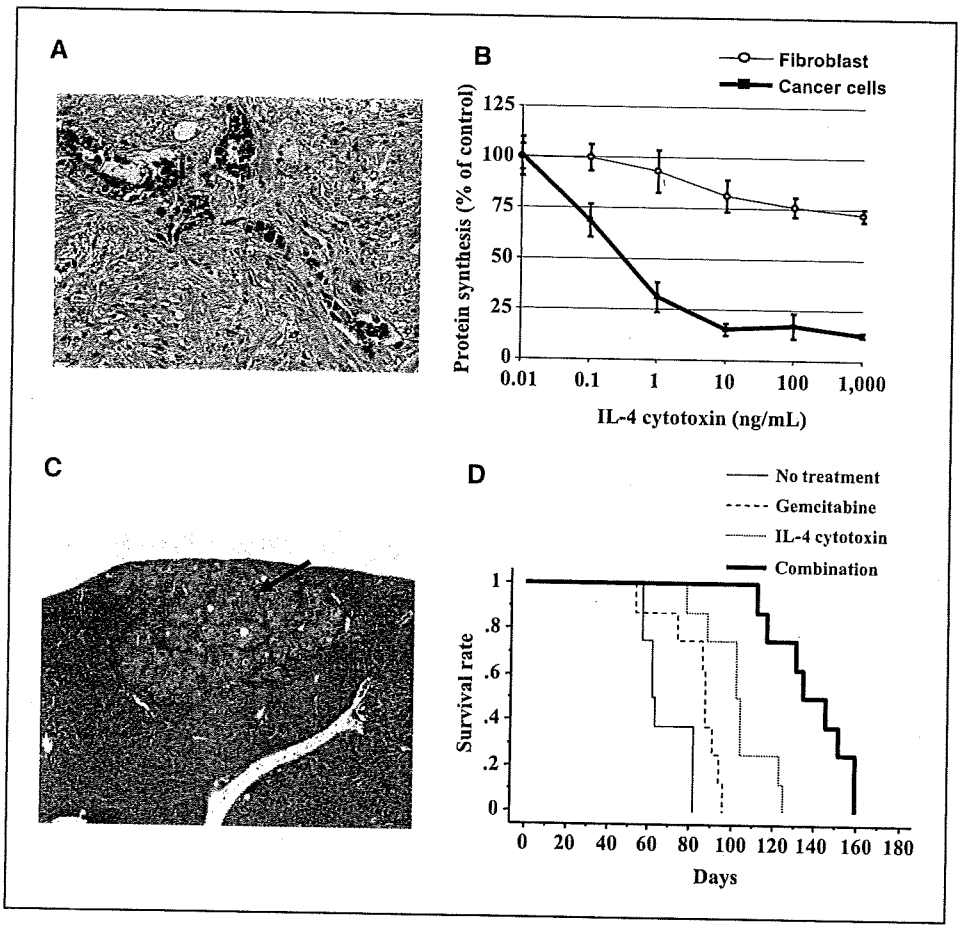

Figure 5. Advanced pancreatic cancer model generated from a clinical sample by orthotopic transplantation in SCID mice. *A*, expression of IL-4Rα in the clinical sample. The tissue specimen was stained with anti-human IL-4Rα polyclonal antibody. Magnification, ×200. *B*, cytotoxic activity of IL-4 cytotoxin (0–1,000 ng/mL) to primary tumor cell and fibroblasts, as determined by protein synthesis inhibition assay. *C*, metastasis lesion to liver (*arrows*) was detected 1 mo after orthotopic transplantation. Magnification, ×40. *D*, Kaplan-Meier survival curves (n = 10 mice) after treatment with gemcitabine (150 mg/kg, twice a week), IL-4 cytotoxin (100 μg/kg, twice a day during days 31–35), and their combination.

including the invasive and metastatic pattern (44). Accordingly, the peritoneal organs, lymph nodes, liver, and spleen of mice in our model showed tumor metastasis and invasion 1 month after transplantation. IL-4 cytotoxin and gemcitabine showed remarkable antitumor effects in this model. In future studies, it will be of interest to determine whether metastatic lesions to various organs express IL-4R, and after treatment with IL-4 cytotoxin these receptor levels decrease along with disappearing tumor. In other orthotopic tumor model, tumor pieces developed from MIPaCa-2-GFP cells by s.c. is implanted to pancreas of nude mice. In this model, IL-4 cytotoxin as well as gemcitabine caused profound antitumor effects. These data are compatible with our previous report that showed the survival benefit by IL-4 cytotoxin alone in orthotopic early and advanced animal models using Panc-1 and BxPC-3 pancreatic cancer cell lines (19). Although we did not test IL-4R–negative tumor *in vivo* models, our previous studies have shown that non–small cell lung cancer cell line expressing no or low IL-4R are not sensitive to IL-4 cytotoxin *in vivo* (20). Similar conclusions were drawn in squamous cell carcinoma of head and neck tumor models (45). Thus, IL-4 cytotoxin and gemcitabine show better survival benefit compared with either agent alone in two pancreatic tumor models, one derived from clinical sample and the other derived from MIPaCa-2 cell line.

The whole-body imaging of host visualizes the real-time tumor growth at the primary site and tumor development at metastasis sites without the invasive procedures, surgery, anesthesia, or use of contrast medium. Due to the fact that whole-body imaging has the potential of high correlation with MRI in quantifying tumor volume, the precise evaluation of tumor growth rate, metastatic situation, and effectiveness of drugs could all be monitored without sacrificing animals (32, 46). In addition, imaging may identify biomarker of tumor response in preclinical models that can be validated in the clinical trial (47). A recent article reported that red fluorescent protein showed brighter and less background image compared with GFP, when animals were imaged (48). In our study, we used GFP-transfected cells. Therefore, it is possible that we were not able to detect micrometastasis lesions. Nevertheless, we could show that mice developed spontaneous tumor metastasis within the short time after orthotopic transplantation, which correlated with short survival time. In addition, our model showed that IL-4 cytotoxin reduced the rate of tumor growth, including primary and metastasis lesions for 15 and 9 days after treatment in early and advanced model, respectively.

Although IL-4 cytotoxin mediated remarkable antitumor effects *in vivo*, no visible signs of toxicity and features such as weight loss and inactivity were observed in mice receiving optimal doses of IL-4 cytotoxin and/or gemcitabine (data not shown). These results are compatible with previous studies related to both agents (data not shown; refs. 19, 24, 49). Previous studies have shown that low-density IL-4R are expressed on normal immunologic and non-hematopoietic cells (22). Consequently, IL-4 cytotoxin is not cytotoxic to these cells. Preclinical toxicity studies in mice have shown that IL-4 cytotoxin is well tolerated up to 475 μg/kg dose given i.v. (50). As human IL-4 does not bind murine IL-4R, IL-4

cytotoxin has also been administered to cynomolgus monkeys, whose IL-4R binds human IL-4. In these animals, IL-4 cytotoxin was reasonably tolerated up to a dose of 200 μg/kg given i.v. every alternate day for three injections (21). In a phase 1 clinical trial, reversible elevation of liver enzymes and injection site inflammatory reactions were reported after i.v. administration of IL-4 cytotoxin at 0.027 mg/m^2 (25). As our study shows synergistic effects when IL-4 cytotoxin is combined with gemcitabine against pancreatic cancer *in vitro* and *in vivo*, lower doses of IL-4 cytotoxin may be effective for the treatment of patients with PDA when combined with gemcitabine.

In conclusion, these studies provide a novel approach for monitoring tumor response by whole-body imaging of the host. Further studies should be done to evaluate the safety, tolerability, and efficacy of IL-4 cytotoxin when combined with gemcitabine in various pancreatic cancer models. In addition, because of their synergistic effect, IL-4 cytotoxin in combination with gemcitabine should be tested in patients with PDA.

Acknowledgments

Received 12/13/2006; revised 5/31/2007; accepted 7/23/2007.

The costs of publication of this article were defrayed in part by the payment of page charges. This article must therefore be hereby marked *advertisement* in accordance with 18 U.S.C. Section 1734 solely to indicate this fact.

We thank Dr. Ming-Sound Tsao (Ontario Cancer Institute/Princess Margaret Hospital University of Toronto, Toronto, Ontario, Canada) for providing the HPDE cell line, Dr. Raymond Donnelly for critical reading of the manuscript, Pamela Dover for technical support, Dr. Satoru Takahashi for his evaluation of immunohistochemistry results, and the Cooperative Human Tissue Network for PDA and normal pancreas tissues.

References

1. Sener SF, Fremgen A, Menck HR, Winchester DP. Pancreatic cancer: a report of treatment and survival trends for 100,313 patients diagnosed from 1985-1995, using the National Cancer Database. J Am Coll Surg 1999;189:1–7.
2. Tempero M, Plunkett W, Ruiz Van Haperen V, et al. Randomized phase II comparison of dose-intense gemcitabine: thirty-minute infusion and fixed dose rate infusion in patients with pancreatic adenocarcinoma. J Clin Oncol 2003;21:3402–8.
3. Burris HA, Moore MJ, Andersen J, et al. Improvements in survival and clinical benefit with gemcitabine as first-line therapy for patients with advanced pancreas cancer: a randomized trial. J Clin Oncol 1997;15:2403–13.
4. Bruns CJ, Solorzano CC, Harbison MT, et al. Blockade of the epidermal growth factor receptor signaling by a novel tyrosine kinase inhibitor leads to apoptosis of endothelial cells and therapy of human pancreatic carcinoma. Cancer Res 2000;60:2926–35.
5. Yokoi K, Sasaki T, Bucana CD, et al. Simultaneous inhibition of EGFR, VEGFR, and platelet-derived growth factor receptor signaling combined with gemcitabine produces therapy of human pancreatic carcinoma and prolongs survival in an orthotopic nude mouse model. Cancer Res 2005;65:10371–80.
6. Bergers G, Song S, Meyer-Morse N, Bergsland E, Hanahan D. Benefits of targeting both pericytes and endothelial cells in the tumor vasculature with kinase inhibitors. J Clin Invest 2003;111:1287–95.
7. Fujioka S, Sclabas GM, Schmidt C, et al. Inhibition of constitutive NF-κB activity by IκB αM suppresses tumorigenesis. Oncogene 2003;22:1365–70.
8. Moore MJ, Goldstein J, Hamm A, et al. Erlotinib plus gemcitabine compared to gemcitabine alone in patients with advanced pancreatic cancer. A phase III trial of the National Cancer Institute of Canada Clinical Trials Group [NCIC-CTG]. J Clin Oncol. 2005 ASCO Annual Meeting Proceedings. Vol 23, No. 16S, Part I of II (June 1 Supplement); 2005:1.
9. Pastan I, Hassan R, Fitzgerald DJ, Kreitman RJ. Immunotoxin therapy of cancer. Nat Rev Cancer 2006;6:559–65.
10. Rand RW, Kreitman RJ, Patronas N, Varricchio F, Pastan I, Puri RK. Intratumoral administration of recombinant circularly permuted interleukin-4-*Pseudomonas* exotoxin in patients with high-grade glioma. Clin Cancer Res 2000;6:2157–65.
11. Weber F, Asher A, Bucholz R, et al. Safety, tolerability, and tumor response of IL4-*Pseudomonas* exotoxin (NBI-3001) in patients with recurrent malignant glioma. J Neurooncol 2003;64:125–37.
12. Kioi M, Husain SR, Croteau D, Kunwar S, Puri RK. Convection-enhanced delivery of interleukin-13 receptor-directed cytotoxin for malignant glioma therapy. Technol Cancer Res Treat 2006;5:239–50.
13. Kreitman RJ, Squires DR, Stetler-Stevenson M, et al. Phase I trial of recombinant immunotoxin RFB4(dsFv)-PE38 (BL22) in patients with B-cell malignancies. J Clin Oncol 2005;23:6719–29.
14. Nelms K, Keegan AD, Zamorano J, Ryan JJ, Paul WE. The IL-4 receptor: signaling mechanisms and biologic functions. Annu Rev Immunol 1999;17:701–38.
15. Toi M, Bicknell R, Harris AL. Inhibition of colon and breast carcinoma cell growth by interleukin-4. Cancer Res 1992;52:275–9.
16. Topp MS, Papadimitriou CA, Eitelbach F, et al. Recombinant human interleukin 4 has antiproliferative activity on human tumor cell lines derived from epithelial and nonepithelial histologies. Cancer Res 1995;55:2173–6.
17. Stadler WM, Rybak ME, Vogelzang NJ. A phase II study of subcutaneous recombinant human interleukin-4 in metastatic renal cell carcinoma. Cancer 1995;76:1629–33.
18. Husain SR, Kreitman RJ, Pastan I, Puri RK. Interleukin-4 receptor-directed cytotoxin therapy of AIDS-associated Kaposi's sarcoma tumors in xenograft model. Nat Med 1999;5:817–22.
19. Kawakami K, Kawakami M, Husain SR, Puri RK. Targeting interleukin-4 receptors for effective pancreatic cancer therapy. Cancer Res 2002;62:3575–80.
20. Kawakami M, Kawakami K, Stepensky VA, et al. Interleukin-4 receptor on human lung cancer: a molecular target for cytotoxin therapy. Clin Cancer Res 2002;8:3503–11.
21. Kawakami M, Kawakami K, Puri RK. Interleukin-4 *Pseudomonas* exotoxin chimeric fusion protein for malignant glioma therapy. J Neurooncol 2003;65:15–25.
22. Kawakami K, Kawakami M, Puri RK. Overexpressed cell surface interleukin-4 receptor molecules can be successfully targeted for antitumor cytotoxin therapy. Crit Rev Immunol 2001;21:299–310.
23. Kreitman RJ, Puri RK, Pastan I. A circularly permuted recombinant interleukin 4 toxin with increased activity. Proc Natl Acad Sci U S A 1994;91:6889–93.
24. Kioi M, Takahashi S, Kawakami M, Kawakami K, Kreitman RJ, Puri RK. Expression and targeting of interleukin-4 receptor for primary and advanced ovarian cancer therapy. Cancer Res 2005;65:8388–96.
25. Garland L, Gitlitz B, Ebbinghaus S, et al. Phase I trial of intravenous IL-4 *Pseudomonas* exotoxin protein (NBI-3001) in patients with advanced solid tumors that express the IL-4 receptor. J Immunother 2005;28:376–81.
26. Rainov NG, Heidecke V. Long term survival in a patient with recurrent malignant glioma treated with intratumoral infusion of an IL4-targeted toxin (NBI-3001). J Neurooncol 2004;66:197–201.
27. Hoffman RM. The multiple uses of fluorescent proteins to visualize cancer *in vivo*. Nat Rev Cancer 2005;10:796–806.
28. Furukawa T, Duguid WP, Rosenberg L, Viallet J, Galloway DA, Tsao MS. Long-term culture and immortalization of epithelial cells from normal adult human pancreatic ducts transfected by the E6E7 gene of human papilloma virus 16. Am J Pathol 1996;148:1763–70.
29. Puri RK, Leland P, Kreitman RJ, Pastan I. Human neurological cancer cells express interleukin-4 (IL-4) receptors which are targets for the toxic effects of IL4-*Pseudomonas* exotoxin chimeric protein. Int J Cancer 1994;58:574–81.
30. Chou TC, Motzer R, Tong Y, Bosl G. Computerized quantitation of synergism and antagonism of Taxol, topotecan, and cisplatin against human teratocarcinoma cell growth: a rational approach to clinical protocol design. J Natl Cancer Inst 1994;86:1517–24.
31. Murata T, Obiri NI, Debinski W, Puri RK. Structure of IL-13 receptor: analysis of subunit composition in cancer and immune cells. Biochem Biophys Res Commun 1997;238:90–4.
32. Bouvet M, Wang J, Nardin SR, et al. Real-time optical imaging of primary tumor growth and multiple metastatic events in a pancreatic cancer orthotopic model. Cancer Res 2002;62:1534–40.
33. Abbruzzese JL. Past and present treatment of pancreatic adenocarcinoma: chemotherapy as a standard treatment modality. Semin Oncol 2002;29:2–8.
34. Symon Z, Davis M, McGinn CJ, Zalupski MM, Lawrence TS. Concurrent chemoradiotherapy with gemcitabine and cisplatin for pancreatic cancer: from the laboratory to the clinic. Int J Radiat Oncol Biol Phys 2002;53:140–5.
35. Bocci G, Fioravanti A, Orlandi P, et al. Fluvastatin synergistically enhances the antiproliferative effect of gemcitabine in human pancreatic cancer MIAPaCa-2 cells. Br J Cancer 2005;93:319–30.
36. Pratesi G, Petrangolini G, Tortoreto M, et al. Therapeutic synergism of gemcitabine and CpG-oligodeoxynucleotides in an orthotopic human pancreatic carcinoma xenograft. Cancer Res 2005;65:6388–93.
37. Chun PY, Feng FY, Scheurer AM, et al. Synergistic effects of gemcitabine and gefitinib in the treatment of head and neck carcinoma. Cancer Res 2006;66:981–8.
38. O'Connor R, Liu C, Ferris CA, et al. Anti-B4-blocked ricin synergizes with doxorubicin and etoposide on multidrug-resistant and drug-sensitive tumors. Blood 1995;86:4286–94.
39. Kim CN, Bhalla K, Kreitman RJ, et al. Diphtheria toxin fused to granulocyte-macrophage colony-stimulating factor and Ara-C exert synergistic toxicity against human AML HL-60 cells. Leuk Res 1999;23:527–38.
40. Polito L, Bolognesi A, Tazzari PL, et al. The conjugate Rituximab/saporin-S6 completely inhibits clonogenic growth of CD20-expressing cells and produces a synergistic toxic effect with Fludarabine. Leukemia 2004;18:1215–22.
41. Gilbert JA, Lloyd RV, Ames MM. Lack of mutations in EGFR in gastroenteropancreatic neuroendocrine tumors. N Engl J Med 2005;353:209–10.
42. Morgan A. Recently approved antineoplastic agents. Highlights Oncol Pract 1996;14:74–9.
43. Husain SR, Kawakami K, Kawakami M, Puri RK. Interleukin-4 receptor-targeted cytotoxin therapy of androgen-dependent and -independent prostate

carcinoma in xenograft models. Mol Cancer Ther 2003;2:245–54.
44. Manzotti C, Audisio RA, Pratesi G. Importance of orthotopic implantation for human tumors as model systems: relevance to metastasis and invasion. Clin Exp Metastasis 1993;11:5–14.
45. Strome SE, Kawakami K, Alejandro D, et al. Interleukin 4 receptor-directed cytotoxin therapy for human head and neck squamous cell carcinoma in animal models. Clin Cancer Res 2002;8:281–6.
46. Bouvet M, Spernyak J, Katz MH, et al. High correlation of whole-body red fluorescent protein imaging and magnetic resonance imaging on an orthotopic model of pancreatic cancer. Cancer Res 2005;65:9829–33.
47. Saur D, Seidler B, Schneider G, et al. CXCR4 expression increases liver and lung metastasis in a mouse model of pancreatic cancer. Gastroenterology 2005;129:1237–50.
48. Katz MH, Takimoto S, Spivack D, Moossa AR, Hoffman RM, Bouvet M. A novel red fluorescent protein orthotopic pancreatic cancer model for the preclinical evaluation of chemotherapeutics. J Surg Res 2003;113:151–60.
49. Zhang X, Galardi E, Duquette M, Lawler J, Parangi S. Antiangiogenic treatment with three thrombospondin-1 type 1 repeats versus gemcitabine in an orthotopic human pancreatic cancer model. Clin Cancer Res 2005;11:5622–30.
50. Puri RK, Hoon DS, Leland P, et al. Preclinical development of a recombinant toxin containing circularly permuted interleukin 4 and truncated *Pseudomonas* exotoxin for therapy of malignant astrocytoma. Cancer Res 1996;56:5631–7.

5-Aminosalicylic Acid Given in the Remission Stage of Colitis Suppresses Colitis-Associated Cancer in a Mouse Colitis Model

Ikuko Ikeda,[1] Ayako Tomimoto,[1] Koichiro Wada,[3] Toshio Fujisawa,[1] Koji Fujita,[1] Kyoko Yonemitsu,[1] Yuichi Nozaki,[1] Hiroki Endo,[1] Hirokazu Takahashi,[1] Masato Yoneda,[1] Masahiko Inamori,[1] Kensuke Kubota,[1] Satoru Saito,[1] Yoji Nagashima,[2] Hitoshi Nakagama,[4] and Atsushi Nakajima[1]

Abstract **Purpose:** The risk of colorectal cancer is increased in patients with inflammatory bowel diseases, especially those with ulcerative colitis (UC). Although 5-aminosalicylic acid (5-ASA) is widely used in the treatment of UC to suppress the colitic inflammation, no studies have been conducted to examine the chemopreventive effect of 5-ASA, given in the remission phase of colitis, against colitis-associated cancer using animal models. We therefore investigated the possible inhibition by peroxisome proliferator-activated receptor-γ (PPARγ) ligands and 5-ASA of colitis-associated colon carcinogenesis in a mouse model.

Experimental Design: A dextran sodium sulfate/azoxymethane–induced mouse colon cancer model was used, and the chemopreventive effects of 5-ASA and PPARγ ligands, given in the remission phase of colitis, against colitis-related colon carcinogenesis, were evaluated.

Results: The number of neoplasms in the mice treated with 5-ASA was significantly lower than that in the control mice. In addition, the size of the neoplasms in treated mice was also significantly smaller than that in the control mice. In contrast, no significant suppression in the number or size of the tumors was observed in the mice treated with PPARγ ligands. The proliferating cell nuclear antigen–labeling index in the tumor cells of the 5-ASA–treated mice was significantly smaller than that in the control, indicating that 5-ASA reduced tumor cell proliferation.

Conclusion: Our results revealed that 5-ASA given in the remission phase of colitis significantly suppressed the development of colitis-associated cancer in a mouse model, which indicates the clinical importance of adopting chemopreventive strategies even in UC patients in remission.

In recent decades, the prevalence of inflammatory bowel disease, i.e., ulcerative colitis (UC) and Crohn's disease has been increasing annually throughout the world. One possible reason is that patients with inflammatory bowel disease survive longer than before because of advances in treatments. On the other hand, the risk of colorectal cancer in these patients, so-called colitis-associated cancer, has also increased, especially in cases of UC. Colitis-associated cancer is believed to be a result of chronic inflammation. A recent meta-analysis has estimated the incidence rate of colitis-associated cancer at 7 per 1,000 person-years and 12 per 1,000 person-years in the second and third decades of UC, respectively (1). Therefore, attempts at prevention of colitis-associated cancer in this high-risk group of patients are considered to be important.

Recent clinical reports have suggested that treatment of UC patients with 5-aminosalicylic acid (5-ASA) might reduce the incidence of colitis-associated cancer (2, 3). Although these reports suggest that treatment of UC patients with 5-ASA may be useful for the prevention of colitis-associated cancer, the precise chemopreventive effects have not been elucidated yet. Therefore, it is considered important that the chemopreventive effect of 5-ASA and the mechanisms underlying the chemoprevention of colitis-associated cancer by 5-ASA have been investigated using animal models. Although 5-ASA is widely used in the treatment of UC to suppress colonic inflammation, no studies have been conducted to examine the chemoprevention by 5-ASA, given in the remission phase of colitis, against colitis-associated cancer using animal models. In addition, the pathogenesis of inflammatory bowel disease–related colitic cancer is still unclear, although various studies using animal

Authors' Affiliations: [1]Gastroenterology Division, [2]Department of Pathology, Yokohama City University Graduate School of Medicine, Yokohama, Japan, [3]Department of Pharmacology, Graduate School of Dentistry, Osaka University, Osaka, Japan, and [4]Biochemistry Division, National Cancer Center Research Institute, Tokyo, Japan

Received 5/16/07; revised 7/24/07; accepted 8/2/07.

Grant support: Program for Promotion of Fundamental Studies in Health Sciences of the National Institute of Biomedical Innovation, a Grant-in-Aid from the Ministry of Health, Labour, and Welfare of Japan (A. Nakajima), a grant (Kiban B) from the Ministry of Education, Culture, Sports, Science, and Technology, Japan (A. Nakajima), a grant from the Human Science Foundation (A. Nakajima), and a Princess Takamatsu Cancer Research Fund (A. Nakajima).

The costs of publication of this article were defrayed in part by the payment of page charges. This article must therefore be hereby marked *advertisement* in accordance with 18 U.S.C. Section 1734 solely to indicate this fact.

Note: Supplementary data for this article are available at Clinical Cancer Research Online (http://clincancerres.aacrjournals.org/).

I. Ikeda and A. Tomimoto contributed equally to this article.

Requests for reprints: Atsushi Nakajima, Gastroenterology Division, Yokohama City University Graduate School of Medicine, 3-9 Fuku-ura, Kanazawa-ku, Yokohama 236-0004, Japan. Phone: 81-45787-2640; Fax: 81-45787-8988; E-mail: nakajima-tky@umin.ac.jp.

doi:10.1158/1078-0432.CCR-07-1208

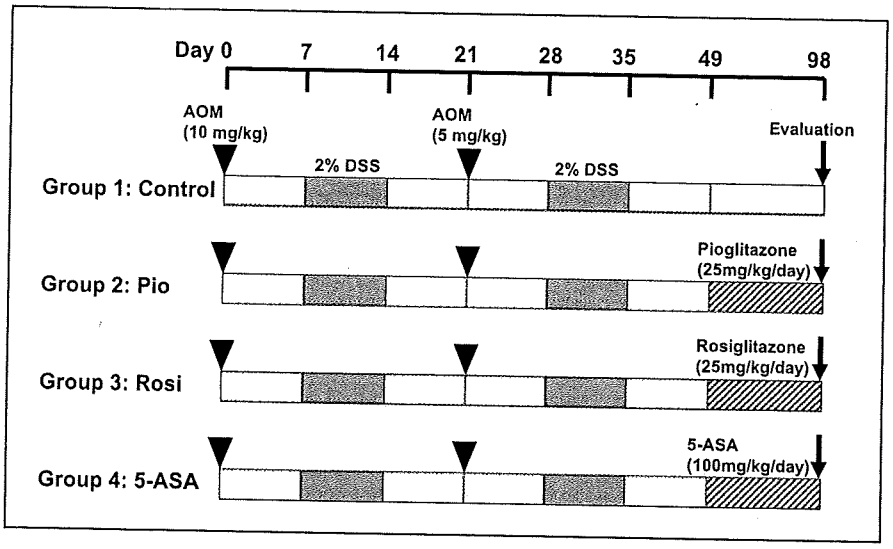

Fig. 1. Experimental protocol for investigating the chemopreventive effects of PPARγ ligands and 5-ASA in a mouse model of colitic cancer. Group 1: Control, 1 wk after the first i.p. azoxymethane (10 mg/kg) injection, the mice were given 2% DSS in drinking water for 7 d, then 1 wk after the second i.p. azoxymethane (5 mg/kg) injection, the mice were again given 2% DSS in the drinking water for 7 d. Group 2: Pio, treated with pioglitazone (25 mg/kg). Group 3: Rosi, treated with rosiglitazone (25 mg/kg). Group 4: 5-ASA, treated with 5-ASA (100 mg/kg).

models have been conducted to investigate the pathogenesis (4–6). Dextran sodium sulfate (DSS) is the most widely used chemical to induce colitis (6), and the DSS-induced colitis model is also expected to be useful for the study of inflammatory bowel disease–related colitis-associated cancer. A relationship between the severity of DSS-induced inflammation and colorectal carcinogenesis, similar to that between human UC-associated dysplasia and the cancer histopathology, has been reported (5). However, the development of these DSS-induced colitis-associated cancer models need long experimental periods or repeated administration of DSS (5). In contrast, several groups have reported that exposure of mice to a single dose of azoxymethane followed by 1 week's treatment with 2% DSS could induce colonic epithelial malignancy after 6 to 20 weeks. Therefore, the azoxymethane/DSS experimental animal models are useful models for the investigation of carcinogenesis in human UC patients.

Previously, our group reported that peroxisome proliferator–activated receptor γ (PPARγ) ligands reduced colorectal tumor formation in a mouse model of colon carcinogenesis (7). PPARγ, a nuclear hormone receptor, serves as a strong link between lipid metabolism and the regulation of gene transcription (8). PPARγ is known to regulate growth arrest and terminal differentiation of adipocytes (9). In addition, PPARγis expressed in various organs, including adipose tissue, breast epithelium, small intestine, lungs, and colon (10), and is also up-regulated in various types of cancer cells. Therefore, we conducted this study to investigate whether PPARγ ligands and 5-ASA might inhibit colitis-associated colon carcinogenesis using the DSS/azoxymethane–induced mouse colon cancer model: we evaluated the chemopreventive effects on colitis-related colon carcinogenesis in the remission stage after the induction of colitis, although in many previous studies, the drugs were given before the induction of colitis.

Materials and Methods

Chemicals and animals. All mice were treated humanely in accordance with the NIH and AERI-BBRI Animal Care and Use Committee guidelines. All animal experiments were approved by the Institutional Animal Care and Use Committee of Yokohama City University School of Medicine. Five-week-old Crj:CD-1 (ICR-1) male mice were purchased from Charles River Japan, Inc. Azoxymethane was purchased from Sigma. DSS with a molecular weight of 40,000 was purchased from MP Biomedicals. The two different PPARγ ligands, pioglitazone and rosiglitazone, were kindly provided by Takeda Chemical Industries, Ltd. (Tokyo, Japan) and GlaxoSmithKline (BN, United Kingdom), respectively. 5-ASA was kindly provided by Nisshin Kyorin Pharmaceutical Co., Ltd. (Tokyo, Japan). The dose levels of the PPARγ ligands were determined on the basis of the results of our previous studies (7).

Induction of colitis-associated cancer in the mouse model. Male ICR-1 mice were given a first i.p. injection of azoxymethane (10 mg/kg) on day 0 (see Fig. 1). Seven days after the azoxymethane injection, the mice were given 2% DSS in the drinking water for 7 days. One week after the discontinuation of DSS administration, the mice were given a second i.p. injection of azoxymethane (5 mg/kg). Then, 7 days after the second azoxymethane injection, the mice were again given 2% DSS in the drinking water for 7 days. Two weeks later, the mice were randomly divided into four groups: group 1 was fed a diet without PPARγligands or 5-ASA; groups 2 to 4 were fed diets with the PPARγligands pioglitazone (25 mg/kg, group 2) or rosiglitazone (25 mg/kg, group 3), or 5-ASA (100 mg/kg, group 4) for 49 days until sacrifice. All mice were sacrificed at the end of the study (day 98; Fig. 1).

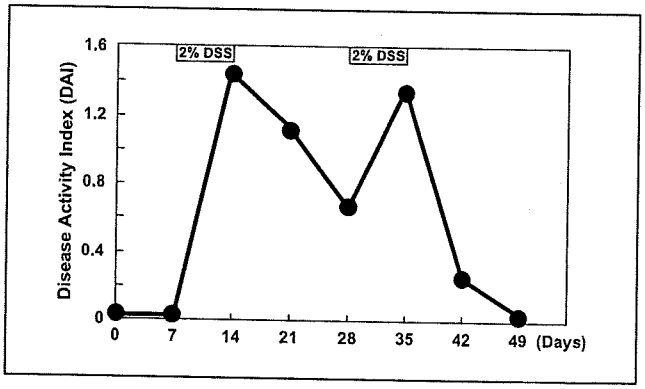

Fig. 2. The disease activity index (*DAI*) was estimated according to the method described. The disease activity increased dramatically immediately after the DSS treatment, to decrease again by 1 wk after the second treatment with DSS.

Table 1. Number and size of tumors

Group	*n*	Body weight (g)	No. of tumors	No. of tumors/mouse	Size of tumors (mm)
(1) Control	8	39.0 ± 1.3*	70	8.5 ± 4.0*	3.3 ± 1.5*
(2) Pioglitazone	6	40.8 ± 1.0*	57	9.5 ± 4.0*	3.6 ± 2.1*
(3) Rosiglitazone	6	39.5 ± 2.4*	58	8.8 ± 4.9*	3.8 ± 1.8*
(4) 5-ASA	8	40.0 ± 4.7*	38	4.0 ± 2.8*	2.4 ± 1.1*

NOTE: A total of 33 male ICR-1 mice were divided into control and experimental groups. The body weights of the mice did not change significantly. As clearly shown, 5-ASA suppressed the formation of neoplasms ($P < 0.05$). The size of the neoplasms in the colon of mice fed the diet containing 5-ASA was smaller than that in the colon specimens from other groups ($P < 0.01$).
*Mean ± SD.

Assessment of colitis. Body weight, the presence of blood in the feces, and stool consistency were recorded daily for each animal. These variables were used to calculate the average daily disease activity index for each animal, as previously described (11). The disease activity index has been shown to be well-correlated with the colon tissue damage score.

Histopathologic analysis. The histopathologic alterations in the colon were examined on H&E-stained sections. A pathologist (Y. Nagashima) diagnosed the colonic neoplasms according to a previously described method (12).

Immunohistochemistry. Immunohistochemistry for proliferating cell nuclear antigen (PCNA) and β-catenin was done. For PCNA immunohistochemistry, we used a PCNA staining kit (ZYMED Laboratories) in accordance with the manufacturer's instructions. For β-catenin immunohistochemical analysis, we used a monoclonal antibody directed against β-catenin (1:1,200 dilution; BD Transduction Laboratories) and a Vectastain ABC kit (Vector Laboratories).

The PCNA labeling index was expressed as the percentage of cells showing positive staining for PCNA relative to the total number of cells. At least five representative areas in a section were selected by light microscope examination at 400-fold magnification and a minimum of 3,000 tumor cells were counted (13).

Statistical analysis. Statistical analysis of the changes in the body weights of the mice, number of neoplasms, and size of neoplasms were done using a χ^2 test. Differences were considered significant when at $P < 0.05$.

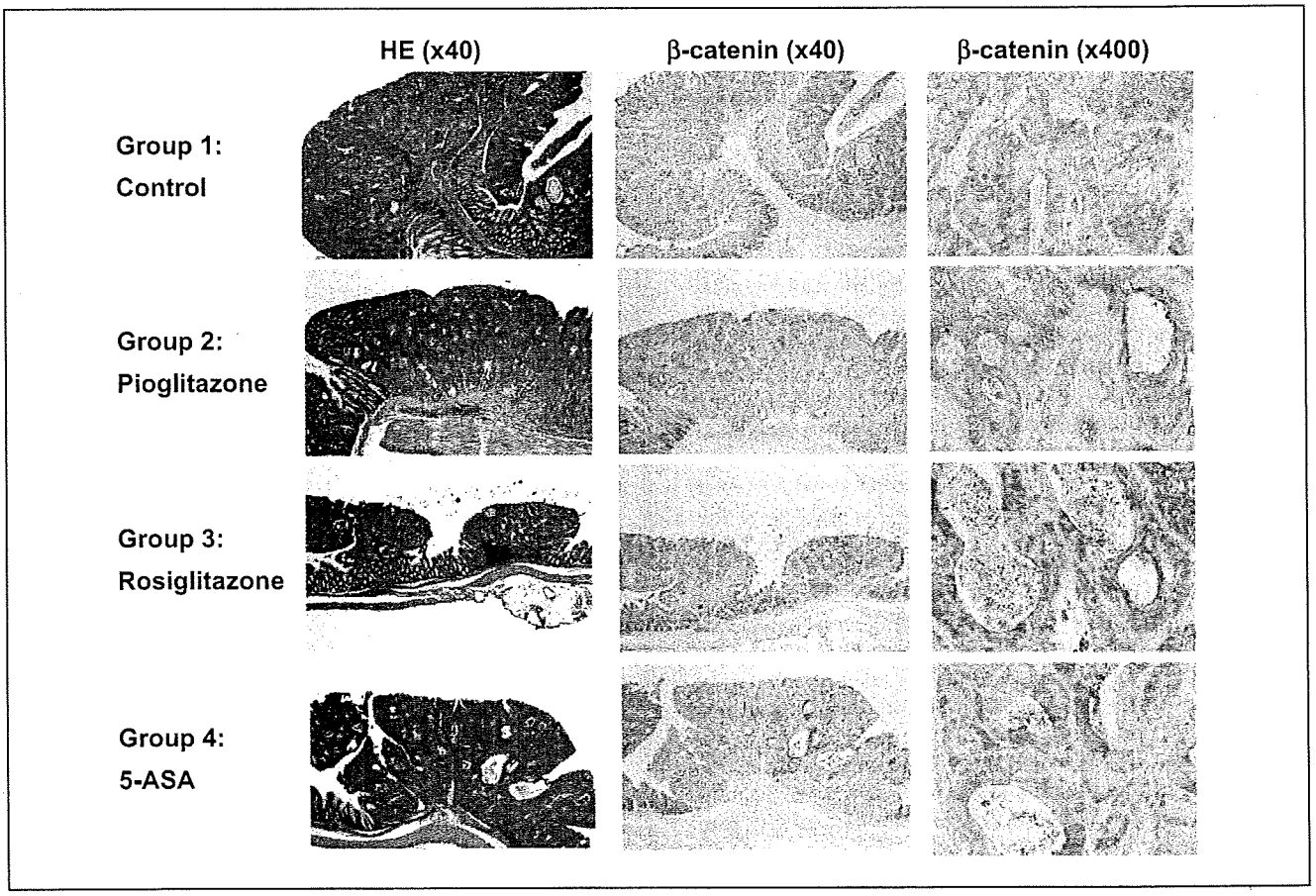

Fig. 3. Microscopic examination of H&E-stained colon sections and β-catenin staining of the tumors. Left, H&E staining (original magnification, ×40). Middle, β-catenin staining (original magnification, ×40). Right, β-catenin staining (original magnification, ×400).

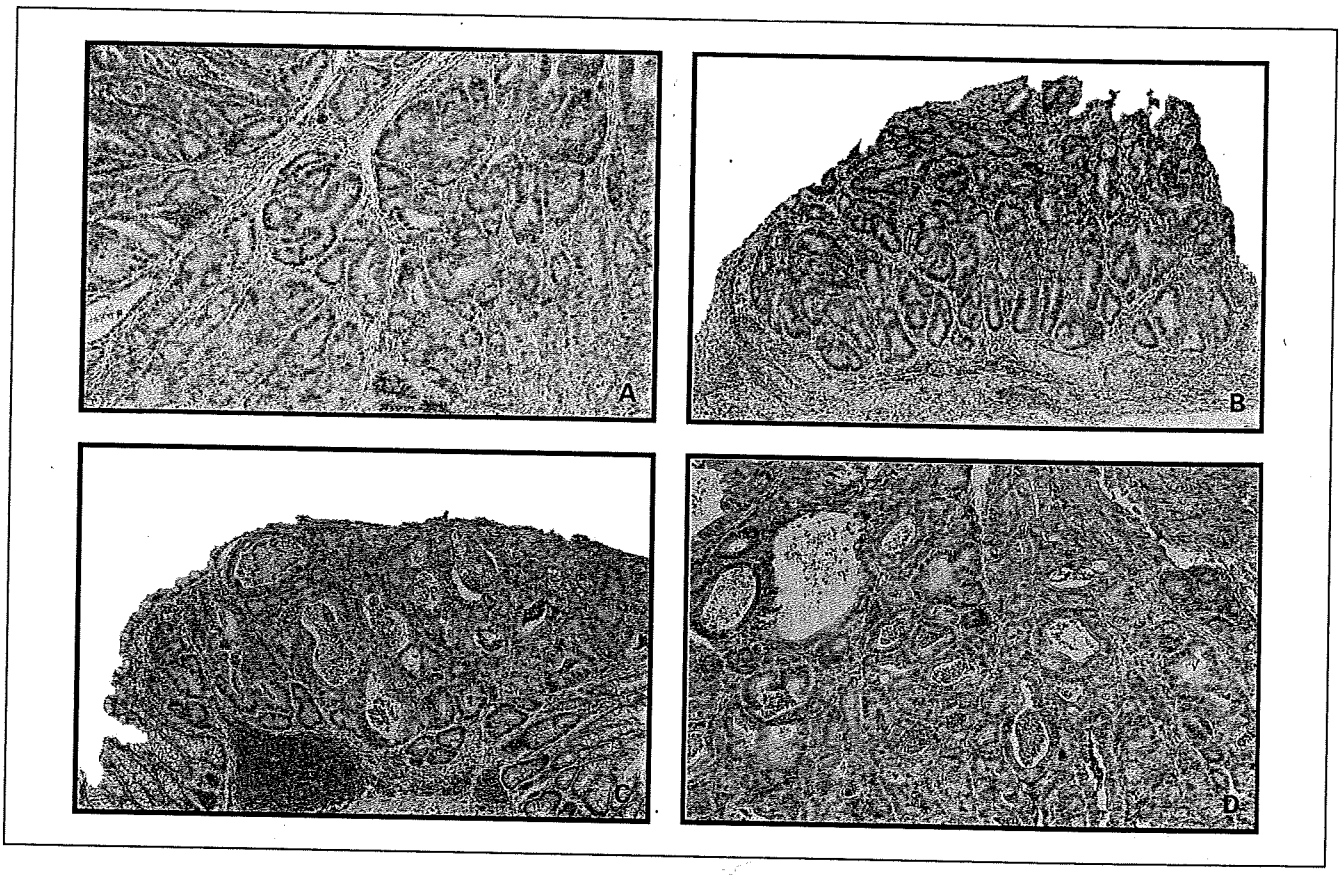

Fig. 4. Immunohistochemistry of PCNA in the tumor cells. *A*, control; *B*, pioglitazone treatment; *C*, rosiglitazone treatment; and *D*, 5-ASA treatment, respectively (original magnification, ×100).

Results

Disease activity index and body weight changes. The disease activity index was estimated according to the method described previously (11). The disease activity increased dramatically immediately after DSS treatment, to decrease again by 1 week after the second treatment with DSS (Fig. 2). The body weights of the mice measured at the end of the study period are shown in Table 1. No significant changes in the mean body weights of the mice was observed in any of the groups.

5-ASA, but not the PPARγ ligands, suppressed tumor formation in the azoxymethane/DSS mice. The number and size of the tumors in the colon specimens obtained from the mice of each group at the end of the study period are shown in Table 1. The number of neoplasms in the colon specimens from the mice treated with 5-ASA (group 4) was significantly lower than that in the colon of the control animals (group 1, $P < 0.05$). In addition, the size of the neoplasms in the colon specimens of the mice treated with 5-ASA were significantly smaller than that in the colon of the control mice. In contrast, no significant decrease of the tumor number and size was observed in the colon specimens from the mice treated with the PPARγ ligands.

Pathologic findings. H&E-stained sections of the tumors from all the groups are shown in Fig. 3. Macroscopically, nodular, polypoid tumors were observed in the middle and distal colon in all the groups. No differences in the morphologic characteristics of the tumors were observed among the groups.

Immunohistochemistry for PCNA and β-catenin. The PCNA labeling index (normal epithelial cells and tumor cells) values are shown in Table 2. The PCNA labeling index in the epithelial cells did not differ significantly among the groups ($P > 0.05$; Supplementary Figure). However, the PCNA labeling index in

Table 2. PCNA labeling index in the colon epithelial cells and tumor cells

Group no., treatment	PCNA-labeling index	
	Non-tumor cells (%)	Tumor cells (%)
(1) Control	26.10 ± 5.31*	45.29 ± 8.02*
(2) Pioglitazone	20.94 ± 8.08*	41.32 ± 8.21*
(3) Rosiglitazone	18.25 ± 2.40*	48.20 ± 11.26*
(4) 5-ASA	23.04 ± 6.34*	30.60 ± 6.61*

NOTE: The PCNA labeling index is expressed as the percentage of cells showing positive staining for PCNA relative to the total number of cells examined. At least five representative areas in a section were selected by light-microscopic examination at 400-fold magnification and a minimum of 3,000 tumor cells were counted. No significant differences in the PCNA labeling index of non-tumor cells was observed among the groups ($P > 0.05$). 5-ASA significantly decreased the PCNA labeling index in the tumor cells ($P < 0.05$).
*Mean ± SD.

the tumor cells in group 4 (5-ASA treatment), but not groups 2 or 3 (treated with the PPARγ ligands), was significantly smaller than that in group 1 (control, $P < 0.05$). Typical microscopic photographs are shown in Fig. 4. Strong β-catenin expression was seen in the nucleus and cytoplasm of the tumor cells, but there were no significant differences among the tumors in the four groups (Fig. 3, *middle* and *right*).

Discussion

In the present study, we clearly showed the chemopreventive effect of 5-ASA against colitis-associated cancer in the remission stage. In contrast, the PPARγ ligands showed no suppressive effect against neoplasm formation. Previously, our group and others have reported that the PPARγ ligands effectively inhibited the colonic inflammation associated with DSS administration, trinitrobenzene sulfonic acid–induced colitis, as well as aberrant crypt foci formation in many animal models (5, 14, 15). However, most of these reports examined the preventive effect of PPARγ ligand therapy, i.e., the PPARγ ligands were given before the induction of inflammation (pretreatment). In the present study, we gave the PPARγ ligands and 5-ASA 2 weeks after the end of DSS treatment. Therefore, all mice were in the remission stage after the induction of colitis. The remission stage was also confirmed by the disease activity index, as shown in Fig. 2 and in the Supplementary Table. As PPARγ ligands have antiinflammatory actions, their antitumor effects against colitis-associated cancer shown in previous studies might be the result of their antiinflammatory effects in colitis-associated cancer (16). This might also be the reason why the PPARγ ligands showed no suppressive effect against tumor development in our present study.

In the present study, 5-ASA markedly suppressed the development of colitic cancer. Although the PCNA labeling index in the non–tumor colonic epithelium did not differ significantly among the groups, only 5-ASA alone significantly suppressed the PCNA labeling index in the tumor cells. These results suggest that 5-ASA may reduce tumor cell but not normal epithelial cell proliferation. Further investigations will be required to clarify the detailed mechanisms.

In conclusion, we found that only 5-ASA given in the remission stage of colitis significantly suppressed the development of colitis-associated cancer in a mouse model. Our results showed the clinical importance of adopting a chemopreventive strategy in UC patients in remission.

References

1. Eaden JA, Abrams KR, Mayberry JF. The risk of colorectal cancer in ulcerative colitis: a meta-analysis. Gut 2001;48:526–35.
2. Bernstein CN, Eaden J, Steinhart AH, Munkholm P, Gordon PH. Cancer prevention in inflammatory bowel disease and the chemoprophylactic potential of 5-aminosalicylic acid. Inflamm Bowel Dis 2002;8:356–61.
3. Rubon DT, Lashner BA. Will a 5-ASA a day keep the cancer (and dysplasia) away? Am J Gastroenterol 2005;100:1345–53.
4. Seril DN, Liao J, Yang CS. Oxidative stress and ulcerative colitis-associated carcinogenesis: studies in humans and animal models. Carcinogenesis 2003;24:353–62.
5. Cooper HS, Murthy S, Kido K, Yoshitake H, Flanigan A. Dysplasia and cancer in the dextran sulfate sodium mouse colitis model. Relevance to colitis-associated neoplasia in the human: a study of histopathology, β-catenin and p53 expression and the role of inflammation. Carcinogenesis 2000;21:757–68.
6. Suzuki R, Kohno H, Sugie S, Tanaka T. Sequential observations on the occurrence of preneoplastic and neoplastic lesions in mouse colon treated with azoxymethane and dextran sodium sulfate. Cancer Sci 2004;95:721–7.
7. Osawa E, Nakajima A, Wada K, et al. Peroxisome proliferator-activated receptor-γ ligands suppress colon carcinogenesis induced by azoxymethane in mice. Gastroenterology 2003;124:361–7.
8. Forman BM, Tontonoz P, Chen J, Brun RP, Spiegelman BM, Evans RM. 15-Deoxy-δ 12,14-prostaglandin J2 is a ligand for the adipocyte determination factor PPAR γ. Cell 1995;83:803–12.
9. Kubota N, Terauchi Y, Miki H, et al. PPAR γ mediates high-fat diet-induced adipocyte hypertrophy and insulin resistance. Mol Cell 1999;4:597–609.
10. Lefebvre AM, Auwerx J. PPARγ is induced during differentiation of colon epithelium cells. J Endocrinol 1999;162:331–40.
11. Cooper HS, Murthy SN, Shah RS, Sedergran DJ. Clinicopathologic study of dextran sulfate sodium experimental murine colitis. Lab Invest 1993;69:238–49.
12. Ward JM. Morphogenesis of chemically induced neoplasms of the colon and small intestine in rats. Lab Invest 1974;30:505–13.
13. Watanabe I, Toyoda M, Okuda J, et al. Detection of apoptotic cells in human colorectal cancer by two different *in situ* methods: antibody against single-stranded DNA and terminal deoxynucleotidyl transferase-mediated dUTP-biotin nick end-labeling (TUNEL) methods. Jpn J Cancer Res 1999;90:188–93.
14. Tanaka T, Kohno H, Yoshitani S, et al. Ligands for peroxisome proliferators-activated receptors α and γ inhibit chemically induced colitis and formation of aberrant crypt foci in rats. Cancer Res 2001;61:2424–8.
15. Su CG, Wen X, Bailey ST, et al. A novel therapy for colitis utilizing PPAR-γ ligands to inhibit the epithelial inflammatory response. J Clin Invest 1999;104:383–9.
16. Kohno H, Suzuki R, Sugie S, Tanaka T. Suppression of colitis-related mouse colon carcinogenesis by a cox-2 inhibitor and PPAR ligands. BMC Cancer 2005;5:46.

Journal of Viral Hepatitis, 2007, **14**, 600–607 doi:10.1111/j.1365-2893.2006.00836.x

Hepatitis C virus directly associates with insulin resistance independent of the visceral fat area in nonobese and nondiabetic patients

M. Yoneda,[1*] S. Saito,[1*] T. Ikeda,[1] K. Fujita,[1] H. Mawatari,[1] H. Kirikoshi,[1] M. Inamori,[1] Y. Nozaki,[1] T. Akiyama,[1] H. Takahashi,[1] Y. Abe,[1] K. Kubota,[1] T. Iwasaki,[2] Y. Terauchi,[2] S. Togo[3] and A. Nakajima[1] [1]*Division of Gastroenterology,* [2]*Division of Endocrinology and Metabolism,* [3]*Department of Gastroenterological Surgery, Yokohama City University Graduate School of Medicine, Yokohama, Japan*

Received August 2006; accepted for publication October 2006

SUMMARY. Insulin resistance (IR) is known to be associated with the visceral adipose tissue area. Elucidation of the relationship between hepatitis C virus (HCV) and IR is of great clinical relevance, because IR promotes liver fibrosis. In this study, we tested the hypothesis that HCV infection by itself may promote IR. We prospectively evaluated 47 patients with chronic HCV infection who underwent liver biopsy. Patients with obesity, type 2 diabetes mellitus (DM), or a history of alcohol consumption were excluded. IR was estimated by calculation of the modified homeostasis model of insulin resistance (HOMA-IR) index. Abdominal fat distribution was determined by computed tomography. Fasting blood glucose levels were within normal range in all the patients. The results of univariate analysis revealed a significant correlation between the quantity of HCV-RNA and the HOMA-IR ($r = 0.368$, $P = 0.0291$). While a significant correlation between the visceral adipose tissue area and the HOMA-IR was also observed in the 97 control, nondiabetic, non-HCV-infected patients ($r = 0.398$, $P < 0.0001$), no such significant correlation between the visceral adipose tissue area and the HOMA-IR ($r = 0.124$, $P = 0.496$) was observed in the patients with HCV infection. Multiple regression analysis with adjustment for age, gender and visceral adipose tissue area revealed a significant correlation between the HCV-RNA and the HOMA-IR ($P = 0.0446$). HCV is directly associated with IR in a dose-dependent manner, independent of the visceral adipose tissue area. This is the first report to demonstrate the direct involvement of HCV and IR in patients with chronic HCV infection.

Key words: hepatitis C virus, HOMA-IR, insulin resistance, visceral adipose tissue

INTRODUCTION

Currently, approximately 200 million people around the world are chronically infected with the hepatitis C virus (HCV). Chronic HCV infection often leads to hepatic cirrhosis and hepatocellular carcinoma, thus posing a worldwide problem, both from the medical and the socioeconomical aspect [1,2]. Recent epidemiological studies have suggested that HCV infection is associated with an increased risk of development of type 2 diabetes mellitus (DM), and that type 2 DM is more prevalent among patients with chronic HCV infection than in patients with other liver diseases and in the general population, irrespective of whether or not hepatic cirrhosis is present [3–6].

Insulin resistance (IR) plays a primary role in the development of type 2 DM. This is supported by the results of prospective longitudinal studies showing that IR is the best predictor of the development of type 2 DM, preceding its onset by 10–20 years [7–10], and the results of cross-sectional studies showing that IR is a consistent finding in patients with type 2 DM [1,2,11]. Recently, visceral adipose tissue has drawn attention as a source of several bioactive substances, known as adipocytokines, such as adiponectin, leptin, plasminogen activator inhibitor-1 and tumour necrosis factor-α, all of which are thought to contribute to IR. It is also well known that IR is strongly associated with the visceral adipose tissue area, and furthermore, that it is a common

*Both the authors contributed equally to this work.

Abbreviations: HCV, hepatitis C virus; DM, diabetes mellitus; HOMA-IR, homeostasis model assessment of insulin resistance; IR, insulin resistance; ALT, alanine aminotransferase; AST, aspartate aminotransferase; GGT, gamma-glutamyl-transferase; IRI, immunoreactive insulin; VFA, visceral fat area; SFA, subcutaneous fat area.

Correspondence: Atsushi Nakajima, Division of Gastroenterology, Yokohama City University Graduate School of Medicine, 3-9 Fukuura, Kanazawa-ku, Yokohama 236-0004, Japan. Tel.: +81-45-787-2640; Fax: +81-45-787-8988; E-mail: nakajima-tky@umin.ac.jp

feature in patients with obesity, type 2 DM and fatty liver [12]. In view of the strong association between HCV infection and the risk of development of DM, it is important to determine whether HCV infection can predispose to the development of IR even before overt diabetes sets in. The effect of HCV infection on IR depends on the viral genotype; patients infected with the genotype 3 virus have a lower prevalence of IR when compared with those infected with the other viral genotypes, even after adjustment for the effects of body mass index (BMI) and other confounders [13,14]. On the other hand, despite the lower prevalence of IR, subjects with HCV genotype 3 infection have more extensive hepatic steatosis [15–17]. Animal studies using transgenic mice carrying the core gene of HCV have suggested that HCV-encoded proteins might alter insulin signalling, thereby causing impaired insulin sensitivity and glycaemia dysregulation [18]. However, the pathogenesis of HCV-associated IR in humans remains to be clearly elucidated. None of the epidemiological studies conducted until now have analysed the relationship between HCV infection and the risk of IR independent of the influence of obesity, type 2 diabetes mellitus or alcohol consumption; therefore, the precise relationship between HCV and IR remains unclear in patients with HCV.

In this study, we tested the hypothesis that in Japanese nondiabetic, nonobese patients without a history of alcohol consumption having chronic HCV infection not caused by HCV genotype 3, the HCV infection by itself may promote IR independent of the visceral adipose tissue area, by determining the degree of IR in the subjects based on the fasting blood glucose and plasma insulin levels, and the homeostasis model assessment of IR (HOMA-IR) index.

METHODS

Patients

We prospectively evaluated 47 patients with chronic HCV infection who underwent liver biopsy at Yokohama City University Hospital between January 2005 and December 2005. The study was conducted with the approval of the Ethics Committee of Yokohama City University Hospital. Hepatitis C genotyping was conducted based on the detection of anti-HCV antibodies using the line probe assay (Inno-LiPA HCV II; Innogenesis, Ghent, Belgium), a second-generation reverse hybridization technique. The serum HCV-RNA titres were examined by the Cobas Amplicor HCV monitor assay (version 2.0) (Roche, Tokyo, Japan) method, with a lower limit of quantitation of 5000 IU /mL and upper limit of quantitation of 5 000 000 IU /mL. The HCV genotype was determined using type-specific primers from the core region of the HCV genome. None of the patients had any clinical evidence of hepatic decompensation, such as hepatic encephalopathy, ascites, variceal bleeding or elevation of the serum bilirubin levels to beyond twofold of the upper limit of normal. Ninety-seven gender- and age-matched nondiabetic, nonobese, nonalcoholic and non-HCV-infected patients were evaluated as controls.

Patients with the following conditions were excluded: concurrent active hepatitis B virus infection (positive for hepatitis B surface antigen) or autoimmune hepatitis, primary biliary cirrhosis (PBC), sclerosing cholangitis, haemochromatosis, α1-antitrypsin deficiency or Wilson's disease. Patients with obesity (BMI > 25), type 2 DM, or a history of alcohol consumption (20 g/day) were also excluded from the study.

Clinical and laboratory evaluation

The 47 patients with chronic HCV infection finally enrolled in the study were interviewed to determine their current average daily alcohol intake (g/day), i.e. in the previous 6 months, and also their past history of alcohol intake (g/day), i.e. prior to the previous 6 months. A current or past history of daily alcohol intake of more than 20 g/day represented a criterion for exclusion from the study. The weight and height of the patients were measured with a calibrated scale.

Venous blood samples were drawn from the patients after overnight (12 h) fasting to determine the serum levels of albumin, alanine aminotransferase (ALT), aspartate aminotransferase (AST) and gamma-glutamyl-transferase (GGT), plasma levels of glucose and insulin, and the platelet count. The plasma insulin level was measured by radioimmunoassay, and the other biochemical analyses were conducted in a conventional automated analyser.

Insulin resistance was calculated by the modified homeostasis model assessment of insulin resistance (HOMA-IR) method using the following formula: HOMA-IR = fasting insulin (μU/mL) × plasma glucose (mg/dL)/405. HOMA-IR, originally developed by Matthews, has since been modified [19,20]. This index has been shown to be well correlated with the results of the euglycaemic–hyperinsulinemic clamp method of assessment of IR in type 2 DM patients.

Determination of the visceral and subcutaneous fat areas

The abdominal fat distribution in the subjects was determined by computed tomography (CT) with the subjects in the supine position, in accordance with a previously described procedure [21]. The subcutaneous fatty area (SFA) and intra-abdominal visceral fatty area (VFA) were measured at the level of the umbilicus using a standardized method, in terms of the CT number. In brief, a region of interest was defined in the subcutaneous fat layer by tracing its contour on each scan, and the attenuation range for fat tissue was measured in terms of the CT number (in Hounsfield units).

Histopathology

The degree of necroinflammatory activity and fibrosis in the liver biopsy specimens were scored semiquantitatively,

as described by Scheur [22], by two hepatopathologists blinded to the clinical data. The portal or periportal and lobular inflammatory activities were scored from 0 to 4. Fibrosis was scored as follows: F0, no fibrosis; F1, enlarged fibrotic portal tracts; F2, periportal or portal–portal septa, but intact hepatic architecture; F3, architectural distortion, but no obvious cirrhosis; and F4, probable or definite cirrhosis. The degree of steatosis was assessed based on the percentage of hepatocytes containing macrovesicular fat deposits; the grading was conducted as follows: grade 0, no steatosis; grade 1, <33% of hepatocytes affected; grade 2, 33–66% of hepatocytes affected; grade 3, >66% of hepatocytes affected [23].

Statistical analysis

All the data were expressed as mean ± SD, unless otherwise indicated. The relationship between any two variables was analysed by standard correlation analysis conducted using the StatView software, version 5.0 (SAS, Cary, NC, USA). The relationships between the quantity of HCV-RNA, VFA, SFA and other relevant covariates were examined by multiple regression analysis and determination of the standardized correlation coefficients. *P*-values <0.05 were considered to be significant.

RESULTS

Patient characteristics and liver biopsy findings

The baseline characteristics of the 47 patients and the 97 nondiabetic and non-HCV-infected gender- and age-matched control subjects are shown in Table 1. The mean age of the patients was 53.0 ± 2.3 years; 29 (61.7%) were male, and the mean BMI was 23.1 ± 2.6 kg/m^2. The distribution of the histopathological scoring of the inflammatory activity in the liver biopsy specimens was as follows: grade 1, 29 (61.7%) patients; grade 2, 15 (31.9%) patients; grade 3, three (6.4%) patients. The distribution of the severity of fibrosis was as follows: absent, seven (14.9%) patients; stage 1, 20 (40.4%) patients; stage 2, 11 (23.4%) patients; stage 3, nine (19.1%) patients. None of the patients had any evidence of cirrhosis. The distribution of the degree of steatosis in the patients was as follows: absent, 32 (68.1%) patients; stage 1, 8 (17.0%) patients; stage 2, seven (14.9%) patients; none of the patients in the study had stage 3 steatosis (shown in Table 2).

Insulin resistance and HCV infection

To determine the hypothesis that HCV infection may by itself predispose to IR before the onset of overt diabetes independently of the visceral adipose tissue area, we assessed the association of HOMA-IR with the quantity of HCV-RNA and the visceral adipose tissue area.

Table 1 Clinical and biochemical characteristics of patients with HCV infection and control patients

	HCV	Control
Age (years)	53.0 ± 2.3	56.2 ± 14.0
Sex (M:F)	29:18	50:47
Genotype 1:2	28:18	–
Alb. (g/dL)	4.4 ± 0.3	4.4 ± 0.3
AST (U/L)	58.2 ± 31.8	33.8 ± 22.8
ALT (U/L)	80.3 ± 51.0	47.0 ± 43.1
GGT (U/L)	101.1 ± 8.7	71.4 ± 83.2
FBS (mg/dL)	101.1 ± 8.7	107.6 ± 12.7
IRI (μU/mL)	9.8 ± 4.1	8.3 ± 4.0
HOMA-IR	2.48 ± 1.1	2.2 ± 1.1
VFA (cm^2)	79.4 ± 37.4	118.2 ± 55.0
SFA (cm^2)	142.0 ± 75.0	175.5 ± 78.0
BMI	23.1 ± 2.6	25.7 ± 5.0
L/S ratio	1.14 ± 6.2	1.03 ± 0.27
HCV-RNA (kIU/mL)	1693.4 ± 1210.15	–

Data are expressed as mean ± SD.
HOMA-IR, homeostasis model assessment of insulin resistance; AST, aspartate aminotransferase; ALT, alanine aminotransferase; GGT, gamma-glutamyltransferase; VFA, visceral fat area; SFA, subcutaneous fat area; L/S ratio: liver to spleen ratio.

Table 2 Histopathological grading of the changes in the liver biopsy specimens

	Number of patients
Inflammatory activity	
Inflammatory Activity Index	
A0	0
A1	29
A2	15
A3	3
Fibrosis	
Fibrosis Index	
F0	7
F1	20
F2	11
F3	9
F4	0
Steatosis	
Steatosis Index	
0	32
1	8
2	7
3	0

The fasting blood glucose levels were within normal range in all the patients. The results of univariate analysis revealed that while there was no significant correlation between the

quantity of HCV-RNA and the fasting blood glucose ($r = 0.178$, $P = 0.3078$) (Fig. 1a), a significant correlation existed between the quantity of HCV-RNA and the fasting plasma insulin level ($r = 0.347$, $P = 0.0408$) (Fig. 1b). A significant correlation was also found between the quantity of HCV-RNA and the HOMA-IR ($r = 0.368$, $P = 0.0291$) (Fig. 1c). There was no significant correlation between inflammatory activity index and the HOMA-IR (Fig. 3a), and between the fibrosis index and the HOMA-IR (Fig. 3b). These results suggested that neither hepatic inflammation nor fibrosis was responsible for the increase in IR in the patients with HCV infection in our study.

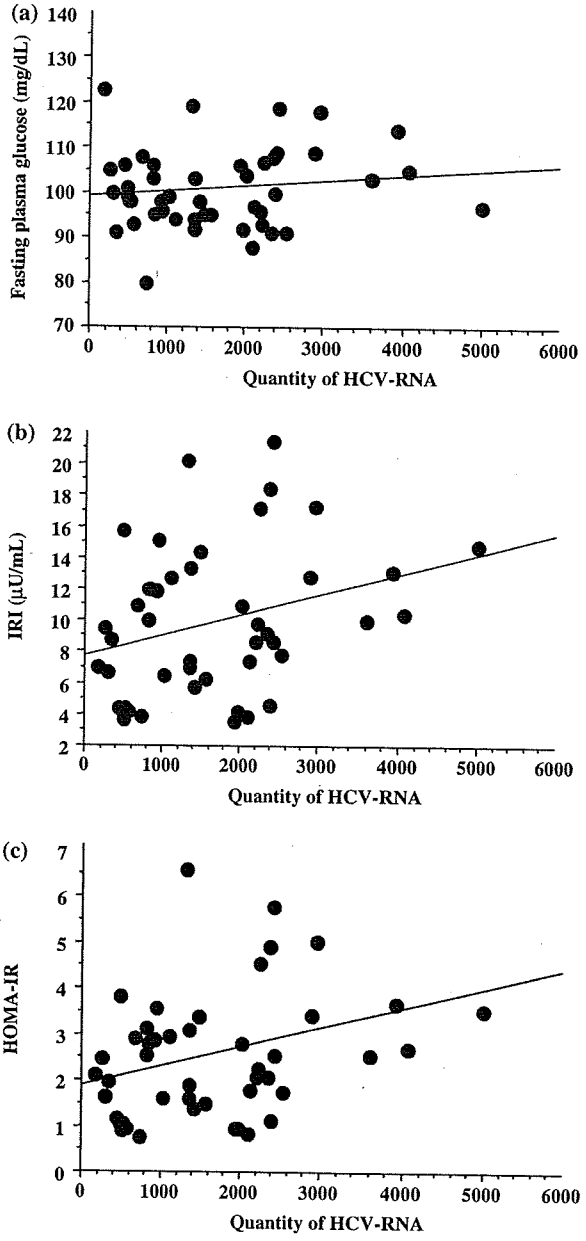

Fig. 1 (a) Correlation between the quantity of HCV-RNA and the fasting blood glucose ($r = 0.178$, $P = 0.3078$). (b) Correlation between the quantity of HCV-RNA and the fasting plasma insulin (IRI: immunoreactive insulin index; $r = 0.347$, $P = 0.0408$). (c) Correlation between the quantity of HCV and the HOMA-IR ($r = 0.368$, $P = 0.0291$).

Visceral adipose tissue may be a major contributor to IR and indeed, there was a significant correlation between the visceral adipose tissue area and the HOMA-IR in the 97 nondiabetic, non-HCV-infected control subjects in this study ($r = 0.398$, $P < 0.0001$) (Fig. 2d). However, to our surprise, we found no significant correlation between the visceral adipose tissue area and the fasting plasma glucose, fasting plasma insulin or the HOMA-IR in the patients with HCV infection in our study [$r = 0.227$, $P = 0.207$ for fasting plasma glucose (Fig. 2a), $r = 0.090$, $P = 0.6218$ for fasting plasma insulin (Fig. 2b) and $r = 0.124$, $P = 0.496$ for HOMA-IR (Fig. 2c)].

Multiple regression analysis

Multiple regression analysis was used to quantify the influence of the measured variables on the HOMA-IR (Table 3). After adjustment for age, gender and visceral adipose tissue area, the quantity of HCV was still significantly correlated with the HOMA-IR ($P = 0.0446$).

DISCUSSION

In this study, we limited our target population to patients with HCV infection not caused by the genotype 3, who were nonobese and nondiabetic and had no history of alcohol consumption. Multiple regression analysis showed that HCV infection was associated with IR in a dose-dependent manner, independent of the other factors considered. As the report by Allison *et al.* [4] of an association between HCV infection and type 2 diabetes, evidence has been accumulating of a possible association between these two conditions. Elucidation of the relationship between HCV and IR would be of great clinical relevance, because IR is known to promote liver fibrosis [24]. Earlier studies which reported increased fasting plasma insulin levels and reduced insulin sensitivity in HCV-infected subjects also included patients with moderate to severe hepatic fibrosis [25,26]. However, more recently, these findings have also been confirmed in HCV-infected patients with minimal or no liver fibrosis [27]. There is one case report of HCV being independently associated with the development of IR after liver transplantation [28]. It has also been reported that HCV infection contributes to the development of IR and increases the long-term risk of development of type 2 DM [27]. Moreover, type 2 diabetes has been reported to be associated with an increased risk of hepatocellular carcinoma [29]. Thus, the results of epidemiological studies have led to a strong suspicion of an association between HCV infection and type 2 diabetes.

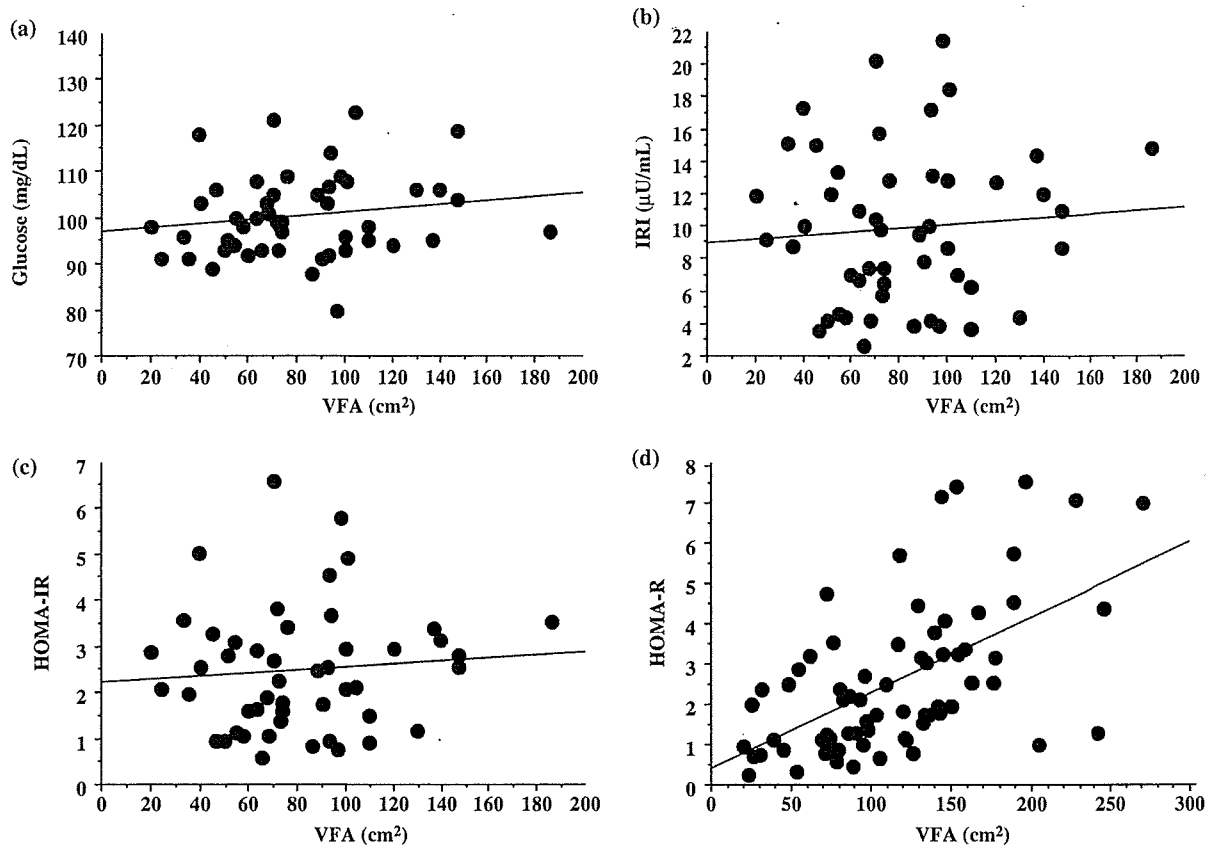

Fig. 2 (a) Correlation between the visceral adipose tissue area and the fasting blood glucose ($r = 0.227$, $P = 0.207$) in patients with HCV infection. (b) Correlation between the visceral adipose tissue area and the fasting plasma insulin (IRI: immunoreactive insulin index; $r = 0.090$, $P = 0.6218$) in patients with HCV infection. (c) Correlation between the visceral adipose tissue area and the HOMA-IR ($r = 0.124$, $P = 0.496$) in patients with HCV infection. (d) Correlation between the visceral adipose tissue area and the HOMA-IR ($r = 0.398$, $P < 0.0001$) in control non-DM, non-HCV-infected patients.

However, there are some difficulties in establishing a definite relationship between HCV infection and type 2 DM on the basis of epidemiological studies, as there are numerous factors in patients that can confound the verification of the existence of a definite relationship, such as obesity, ageing [14], established DM, heavy alcohol consumption, fatty liver and especially, advanced liver injury. None of the epidemiological studies conducted until now has analysed the relationship between HCV infection and the risk of IR independent of the influence of obesity, type 2 DM and alcohol consumption; therefore, the precise relationship between HCV and IR remains unclear. Moreover, the biological mechanism underlying the development of type 2 DM or IR in humans with HCV infection has not been clearly elucidated. On the other hand, animal studies using transgenic mice carrying the core gene of HCV have suggested that HCV-encoded proteins may alter insulin signalling and therefore, tyrosine phosphorylation of insulin receptor substrate (IRS)-1, to explain the impaired insulin sensitivity and glycaemia dysregulation observed in these animals [18]. Moreover, a strong association between IR and the VFA is well known in the non-HCV-infected population [12]. Therefore, we investigated the relationship between HCV infection, IR and VFA in HCV-infected patients without obesity, diabetes or history of alcohol consumption, in order to elucidate the relationship between the quantity of HCV and IR.

In this study, although the fasting plasma glucose levels were within normal limits in all the patients, a significant relationship was found between the quantity of HCV and the fasting plasma level of insulin, and between the quantity of HCV and the HOMA-IR, an indicator of insulin resistance (Fig. 1). Mangia *et al.* [30] reported that they found no association between HCV infection and DM in noncirrhotic patients and that the prevalence of DM in noncirrhotic patients was comparable with that in the general population. However, in their study glucose intolerance was evaluated based on the blood glucose levels, and only patients with levels >126 mg/dL were considered as having abnormal glucose metabolism. Because fasting glucose levels can be

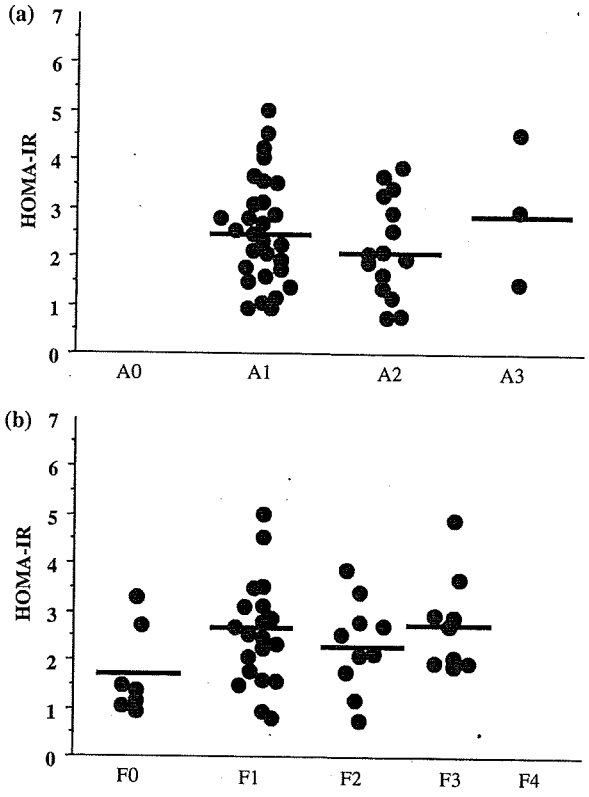

Fig. 3 (a) Correlation between the inflammatory activity index and the HOMA-IR. (b) Correlation between the fibrosis index and the HOMA-IR.

compensated by hyperinsulinaemia, cryptic changes in glucose metabolism should be evaluated by measuring the HOMA-IR. The HOMA model used in this study has been validated and widely used for determining the degree of IR in epidemiological studies. HOMA-IR accounts for approximately 65% of the variability in insulin sensitivity as assessed by the glucose clamp technique [31,32]. It seems to be as good a predictor of clamp-determined insulin sensitivity as the short insulin tolerance test [33].

Abdominal or central fat distribution was first formally recognized to be related to diabetes in 1947 by Vague [34]. Vague's anthropometric observations have since been confirmed in numerous epidemiologic studies [35]. Visceral adipose tissue is a major contributor to IR, and the association between IR and VFA is also well known [36,37]. In our study also, we showed the existence of a significant correlation between the visceral adipose tissue area and the HOMA-IR in our control nondiabetic, non-HCV-infected patients (Fig. 2d). These results were consistent with those reported by Ruderman [36], indicating the reliability of our study. However, to our surprise, no significant correlation was observed in our HCV-infected patients between the visceral adipose tissue area and the HOMA-IR (Fig. 2c). Furthermore, we could not find any significant contribution of hepatic inflammation or fibrosis to the HOMA-IR either (Fig. 3). These results suggest that the IR in HCV-infected patients may be independent of hepatic inflammation or fibrosis.

The results of this study conducted in subjects without a history of DM or obesity suggest that HCV infection increases IR in a dose-dependent manner, independent of the visceral adipose tissue area. Based on the results of our study, we hypothesize that HCV infection by itself may cause IR. Because IR has been reported to play a crucial role in fibrogenesis in chronic hepatitis C infection [38], the presence of chronic HCV infection in addition to a high-fat diet and lack of adequate exercise may be associated with not only an increase of the IR, but also rapid progression of liver fibrosis. Thus, eradication of hepatitis C virus is the ideal treatment for chronic hepatitis C. Recently, combined therapy of this disorder with peg-interferon alpha-2b and ribavirin was shown to elicit a sustained virological response, with a response rate of up to 50%, which represents a very satisfactory response rate to pharmacological treatment [39]. On the other hand, recent studies have demonstrated that IR plays a crucial role in the development of liver fibrosis [38]. Therefore, the results of our study suggest that among cases with failure of virus eradication, reducing the quantity of HCV-RNA may be beneficial for reducing liver fibrosis via promoting normalization of IR. In addition to the anti-viral

Table 3 Multiple regression analysis to determine the relationship between HOMA-IR and other associated variables in the entire study group

Risk factors	Regression coefficient	Standardized regression coefficient	Standard error	*P*-value
Age (year)	0.008	0.026	0.062	0.9022
Gender	−0.184	−0.023	1.756	0.9174
Visceral adipose tissue	−0.017	−0.161	0.022	0.4465
HCV-RNA	0.001	0.431	0.001	0.0446

The dependent variable is the HOMA-IR, and the independent variables are age, gender, visceral adipose tissue and the HCV-RNA titre.
R^2 for the entire model = 0.404.

therapy, addition of oral hypoglycaemic agents for the improvement of IR, such as thiazolidinedione and metformin may greatly contribute to deter the progression of fibrosis.

In conclusion, this is the first report to demonstrate the HCV by itself may be associated with IR in a dose-dependent manner before the development of overt type 2 DM, and IR in patients with HCV infection is independent of the visceral adipose tissue area and the severity of hepatic inflammation or fibrosis. Further clinical studies are necessary to identify the exact pathogenetic roles of HCV in the progression of IR, type 2 DM and liver fibrosis.

ACKNOWLEDGEMENTS

This work supported in part by a Grant-in-Aid from the Ministry of Health, Labor, and Welfare of Japan to AN, a grant (Kiban B) from the Ministry of Education, Culture, Sports, Science and Technology, Japan, to AN, a grant from the National Institute of Biomedical Innovation to AN, and a grant from the Human Science Foundation to AN.

REFERENCES

1 Saito I, Miyamura T, Ohbayashi A *et al.* Hepatitis C virus infection is associated with the development of hepatocellular carcinoma. *Proc Natl Acad Sci U S A* 1990; 87(17): 6547–6549.
2 Simonetti RG, Camma C, Fiorello F *et al.* Hepatitis C virus infection as a risk factor for hepatocellular carcinoma in patients with cirrhosis. A case-control study. *Ann Intern Med* 1992; 116(2): 97–102.
3 Mehta SH, Brancati FL, Sulkowski MS, Strathdee SA, Szklo M, Thomas DL. Prevalence of type 2 diabetes mellitus among persons with hepatitis C virus infection in the United States. *Ann Intern Med* 2000; 133(8): 592–599.
4 Allison ME, Wreghitt T, Palmer CR, Alexander GJ. Evidence for a link between hepatitis C virus infection and diabetes mellitus in a cirrhotic population. *J Hepatol* 1994; 21(6): 1135–1139.
5 el-Zayadi AR, Selim OE, Hamdy H, Dabbous H, Ahdy A, Moniem SA. Association of chronic hepatitis C infection and diabetes mellitus. *Trop Gastroenterol* 1998; 19(4): 141–144.
6 Grimbert S, Valensi P, Levy-Marchal C *et al.* High prevalence of diabetes mellitus in patients with chronic hepatitis C. A case-control study. *Gastroenterol Clin Biol* 1996; 544–548.
7 Warram JH, Martin BC, Krolewski AS, Soeldner JS, Kahn CR. Slow glucose removal rate and hyperinsulinemia precede the development of type II diabetes in the offspring of diabetic parents. *Ann Intern Med* 1990; 113(12): 909–915.
8 Lillioja S, Mott DM, Howard BV *et al.* Impaired glucose tolerance as a disorder of insulin action. Longitudinal and cross-sectional studies in Pima Indians. *N Engl J Med* 1988; 318(19): 1217–1225.
9 Haffner SM, Stern MP, Dunn J, Mobley M, Blackwell J, Bergman RN. Diminished insulin sensitivity and increased insulin response in nonobese, nondiabetic Mexican Americans. *Metabolism* 1990; 39(8): 842–847.
10 Martin BC, Warram JH, Krolewski AS, Bergman RN, Soeldner JS, Kahn CR. Role of glucose and insulin resistance in development of type 2 diabetes mellitus: results of a 25-year follow-up study. *Lancet* 1992; 340(8825): 925–929.
11 Reaven GM, Bernstein R, Davis B, Olefsky JM. Nonketotic diabetes mellitus: insulin deficiency or insulin resistance? *Am J Med* 1976; 60(1): 80–88.
12 Oehler G, Bleyl H, Matthes KJ. Hyperinsulinemia in hepatic steatosis. *Int J Obes* 1982; 6 (Suppl. 1): 137–144.
13 Knobler H, Schihmanter R, Zifroni A, Fenakel G, Schattner A. Increased risk of type 2 diabetes in noncirrhotic patients with chronic hepatitis C virus infection. *Mayo Clin Proc* 2000; 75(4): 355–359.
14 Mason AL, Lau JY, Hoang N *et al.* Association of diabetes mellitus and chronic hepatitis C virus infection. *Hepatology* 1999; 29(2): 328–333.
15 Monto A, Alonzo J, Watson JJ, Grunfeld C, Wright TL. Steatosis in chronic hepatitis C: relative contributions of obesity, diabetes mellitus, and alcohol. *Hepatology* 2002; 36(3): 729–736.
16 Hui JM, Kench J, Farrell GC *et al.* Genotype-specific mechanisms for hepatic steatosis in chronic hepatitis C infection. *J Gastroenterol Hepatol* 2002; 17(8): 873–881.
17 Adinolfi LE, Gambardella M, Andreana A, Tripodi MF, Utili R, Ruggiero G. Steatosis accelerates the progression of liver damage of chronic hepatitis C patients and correlates with specific HCV genotype and visceral obesity. *Hepatology* 2001; 33(6): 1358–1364.
18 Shintani Y, Fujie H, Miyoshi H *et al.* virus infection and diabetes: direct involvement of the virus in the development of insulin resistance. *Gastroenterology* 2004; 126(3): 840–848.
19 Matthews DR, Hosker JP, Rudenski AS, Naylor BA, Treacher DF, Turner RC. Homeostasis model assessment: insulin resistance and beta-cell function from fasting plasma glucose and insulin concentrations in man. *Diabetologia* 1998; 28: 412–419.
20 Levy JC, Matthews DR, Hermans MP. Correct homeostasis model assessment (HOMA) evaluation uses the computer program. *Diabetes Care* 1998; 21: 2191–2192.
21 Yoshizumi T, Nakamura T, Yamane M *et al.* Abdominal fat: standardized technique for measurement at CT. *Radiology* 1999; 211(1): 283–286.
22 Scheuer PJ. Classification of chronic viral hepatitis: a need for reassessment. *J Hepatol* 1991; 13(3): 372–374.
23 Brunt EM. Nonalcoholic steatohepatitis: definition and pathology. *Semin Liver Dis* 2001; 21(1): 3–16.
24 Harrison SA. Steatosis and chronic hepatitis C infection: mechanisms and significance. *Clin Gastroenterol Hepatol* 2005; 3 (10 Suppl. 2): OS92–96.
25 Oncul O, Top C, Cavuplu T. Correlation of serum leptin levels with insulin sensitivity in patients with chronic hepatitis-C infection. *Diabetes Care* 2002; 25(5): 937.
26 Konrad T, Zeuzem S, Toffolo G *et al.* Severity of HCV-induced liver damage alters glucose homeostasis in noncirrhotic patients with chronic HCV infection. *Digestion* 2000; 62(1): 52–59.
27 Hui JM, Sud A, Farrell GC *et al.* Insulin resistance is associated with chronic hepatitis C virus infection and fibrosis progression. *Gastroenterology* 2003; 125(6): 1695–1704.

28 Delgado-Borrego A, Casson D, Schoenfeld D *et al.* virus is independently associated with increased insulin resistance after liver transplantation. *Transplantation* 2004; 77(5): 703–710.
29 Davila JA, Morgan RO, Shaib Y, McGlynn KA, El-Serag HB. Diabetes increases the risk of hepatocellular carcinoma in the United States: a population based case control study. *Gut* 2005; 54(4): 533–539.
30 Mangia A, Schiavone G, Lezzi G *et al.* HCV and diabetes mellitus: evidence for a negative association. *Am J Gastroenterol* 1998; 93(12): 2363–2367.
31 Emoto M, Nishizawa Y, Maekawa K *et al.* Homeostasis model assessment as a clinical index of insulin resistance in type 2 diabetic patients treated with sulfonylureas. *Diabetes Care* 1999; 22(5): 818–822.
32 Bonora E, Targher G, Alberiche M *et al.* Homeostasis model assessment closely mirrors the glucose clamp technique in the assessment of insulin sensitivity: studies in subjects with various degrees of glucose tolerance and insulin sensitivity. *Diabetes Care* 2000; 23(1): 57–63.
33 Bonora E, Moghetti P, Zancanaro C *et al.* Estimates of in vivo insulin action in man: comparison of insulin tolerance tests with euglycemic and hyperglycemic glucose clamp studies. *J Clin Endocrinol Metab* 1989; 68(2): 374–378.
34 Vague J: La differenciation sexualle, facteur determinant des formes de l'obesite. *Presse Med* 1947; 55: 339–340.
35 Ohlson LO, Larsson B, Svardsudd K *et al.* The influence of body fat distribution on the incidence of diabetes mellitus. 13.5 years of follow-up of the participants in the study of men born in 1913. *Diabetes* 1985; 34(10): 1055–1058.
36 Ruderman N, Chisholm D, Pi-Sunyer X, Schneider S. The metabolically obese, normal-weight individual revisited. *Diabetes* 1998; 47(5): 699–713.
37 Katsuki A, Sumida Y, Urakawa H *et al.* Increased visceral fat and serum levels of triglyceride are associated with insulin resistance in Japanese metabolically obese, normal weight subjects with normal glucose tolerance. *Diabetes Care* 2003; 26(8): 2341–2344.
38 Muzzi A, Leandro G, Rubbia-Brandt L *et al.* Insulin resistance is associated with liver fibrosis in non-diabetic chronic hepatitis C patients. *J Hepatol* 2005; 42(1): 41–46.
39 Manns MP, McHutchison JG, Gordon SC *et al.* Peginterferon alfa-2b plus ribavirin compared with interferon alfa-2b plus ribavirin for initial treatment of chronic hepatitis C: a randomised trial. *Lancet* 2001; 358(9286): 958–965.

J Gastroenterol 2007; 42:573–582
DOI 10.1007/s00535-007-2060-x

Journal of Gastroenterology

High-sensitivity C-reactive protein is an independent clinical feature of nonalcoholic steatohepatitis (NASH) and also of the severity of fibrosis in NASH

Masato Yoneda[1], Hironori Mawatari[1], Koji Fujita[1], Hiroshi Iida[1], Kyoko Yonemitsu[1], Shingo Kato[1], Hirokazu Takahashi[1], Hiroyuki Kirikoshi[1], Masahiko Inamori[1], Yuichi Nozaki[1], Yasunobu Abe[1], Kensuke Kubota[1], Satoru Saito[1], Tomoyuki Iwasaki[2], Yasuo Terauchi[2], Shinji Togo[3], Shiro Maeyama[4], and Atsushi Nakajima[1]

[1] Division of Gastroenterology, Yokohama City University Hospital, 3-9 Fuku-ura, Kanazawa-ku, Yokohama 236-0004, Japan
[2] Division of Endocrinology and Metabolism, Yokohama City University Graduate School of Medicine, Yokohama, Japan
[3] Division of Gastroenterological Surgery, Yokohama City University Graduate School of Medicine, Yokohama, Japan
[4] Kitakashiwa Rehabilitation Hospital, Kashiwa, Japan

Background. The changes in nonalcoholic fatty liver disease (NAFLD) range over a wide spectrum, extending from steatosis to steatohepatitis (NASH). However, it has remained difficult to differentiate between NASH and nonprogressive NAFLD by clinical examination. We investigated the interrelationships between serum high-sensitivity C-reactive protein (hs-CRP) and the pathogenesis and progression of NASH. ***Methods.*** Hs-CRP was measured in 100 patients with histologically verified NAFLD (29 with steatosis and 71 with NASH), and a real-time reverse transcriptase-polymerase chain reaction (RT-PCR) analysis was performed to measure the intrahepatic mRNA expressions of CRP and interleukin (IL)-6. ***Results.*** The results of a multiple regression analysis revealed that in comparison with cases of steatosis, hs-CRP was significantly elevated ($P = 0.0048$) in cases of NASH. Furthermore, among patients with NASH, hs-CRP was significantly elevated in those with advanced fibrosis compared with that in those with mild fibrosis ($P = 0.0384$), even after adjustment for age, sex, presence of diabetes, body mass index, visceral fat area, subcutaneous fat area, homeostasis model assessment for insulin resistance, high-density lipoprotein cholesterol, triglyceride, and low-density lipoprotein cholesterol. The results of the RT-PCR analysis showed that intrahepatic mRNA expression of CRP, but not IL-6, was increased in patients with NASH compared with those with steatosis ($P = 0.0228$). ***Conclusions.*** This is the first report to demonstrate consistent and profound elevation of hs-CRP in cases of NASH compared with in cases of simple nonprogressive steatosis. Our results suggest that hs-CRP may be a clinical feature that not only distinguishes NASH from simple nonprogressive steatosis but also indicates the severity of hepatic fibrosis in cases of NASH.

Received: November 26, 2006 / Accepted: March 27, 2007
Reprint requests to: A. Nakajima

Key words: NASH, NAFLD, CRP, fibrosis

Introduction

Nonalcoholic fatty liver disease (NAFLD) is the most common cause of chronic liver injury in many countries around the world.[1,2] NAFLD represents a spectrum of conditions that are histologically characterized by macrovesicular hepatic steatosis, and the diagnosis is made in patients who have not consumed alcohol in amounts considered to be harmful to the liver. The histological changes range over a wide spectrum, extending from simple steatosis, which is generally nonprogressive, to nonalcoholic steatohepatitis (NASH), liver cirrhosis, and liver failure, and sometimes even hepatocellular carcinoma.[3,4] Many clinical laboratory parameters, such as the serum level of adiponectin and homeostasis model assessment for insulin resistance (HOMA-IR) results have been reported to be useful for the diagnosis of NASH. However, until now, it has remained difficult to differentiate between NASH and nonprogressive NAFLD by clinical examination and imaging alone.[5,6] At present, the invasive diagnostic technique of liver biopsy is recognized as the only means to assess the presence and extent of specific necroinflammatory changes and fibrosis necessary for the diagnosis of NASH. Therefore, a noninvasive method for the diagnosis of NASH has been desired.

C-reactive protein (CRP) is one of the major acute-phase proteins and is a marker of systemic inflammation. In contrast to regular CRP assays, a high-sensitivity CRP (hs-CRP) assay enables the diagnosis of even low-grade inflammation. Recently, elevated serum hs-CRP was reported to be a strong predictor of future cardiovascular events.[7–10] Therefore, elucidation of the mechanisms underlying the elevation of the serum hs-CRP

level in healthy subjects is important. It has been suggested that insulin resistance syndrome may be associated with increased serum hs-CRP and visceral obesity.[11,12] Existence of correlation between serum hs-CRP and body mass index (BMI) and waist circumference has also been shown.[12,13] Recent research has yielded compelling evidence to suggest that a wider constellation of disorders may be involved in the metabolic syndrome cluster. These proposed nontraditional components of metabolic syndrome include the presence of subclinical inflammation, microalbuminuria, and, most recently suggested, NAFLD.[14,15] Recently, elevated serum hs-CRP was reported to be a predictor of disease progression in cases of NAFLD.[16–18] We have also previously demonstrated the existence of a significant relationship between serum hs-CRP and risk of disease progression in NAFLD, visceral adipose tissue area, and subcutaneous adipose tissue area in Japanese patients with type 2 diabetes mellitus (DM).[19] However, to date, there is no report of the usefulness of serum CRP to distinguish between patients with NASH and those with nonprogressive simple steatosis.

We were therefore prompted to investigate the potential interrelationship between serum CRP and NASH diagnostic utility.

Patients and methods

Patients

We prospectively evaluated 100 NAFLD patients who underwent liver biopsy at Yokohama City University Hospital between April 2004 to September 2006. The study was conducted with the approval of the Ethics Committee of Yokohama City University.

A detailed history was obtained from all 100 patients, and each underwent a physical examination. Type 2 DM was diagnosed according to World Health Organization criteria.[20] The exclusion criteria included history of hepatic disease such as chronic hepatitis C or concurrent active hepatitis B (serum positive for hepatitis B surface antigen), autoimmune hepatitis, primary biliary cirrhosis, sclerosing cholangitis, hemochromatosis, α1-antitrypsin deficiency, Wilson's disease, or hepatic injury caused by substance abuse, or current or past consumption of more than 20 g of alcohol daily. None of the patients showed any clinical evidence of hepatic decompensation, such as hepatic encephalopathy, ascites, variceal bleeding, or elevation of serum bilirubin level to more than twice the upper limit of normal. Patients with a history of treatment with aspirin or statins were also excluded, because these medications have been suggested to reduce vascular risk among patients with elevated serum CRP,[21–23] as well as patients with a history of treatment with pioglitazone or metformin, which are likely to influence the condition of NASH.[24,25]

Clinical and laboratory evaluation

The weight and height of the patients were measured with a calibrated scale after the patients had removed their shoes and any heavy clothing. Venous blood samples were obtained after the patients had fasted overnight (12 h) for measurement of the serum aspartate aminotransferase (AST), alanine aminotransferase (ALT), glucose, insulin, type IV collagen 7s domain, hyaluronic acid, and hs-CRP concentrations. The serum insulin levels were measured by radioimmunoassay. Other laboratory biochemical parameters were measured in a conventional automated analyzer.

Insulin resistance was calculated by modified HOMA-IR, with the following formula: HOMA-IR = fasting insulin (μU/ml) × plasma glucose (mg/dl)/405. HOMA-IR was originally reported by Matthews DR et al.[26] and has since been modified. This index has been shown to be well correlated with the results of the euglycemic–hyperinsulinemic clamp method to determine insulin resistance in type 2 DM patients. HOMA-IR has been reported to be a suitable method for evaluating the presence of insulin resistance in patients with type 2 diabetes only when their fasting glucose level is <170 mg/dl,[27] and Ono et al.[27] found that the results of HOMA-IR were not significantly correlated with the insulin resistance in subjects with a fasting glucose level >200 mg/dl. Therefore, Type 2 DM patients with poor glycemic control (fasting plasma glucose >170 mg/dl) were excluded from the HOMA-IR measurement.[28]

Determination of the visceral and subcutaneous fat areas

The abdominal fat distribution in the study subjects was determined by computed tomography (CT), conducted with the subjects in the supine position in accordance with a previously described procedure.[29] The subcutaneous fat area (SFA) and intra-abdominal visceral fat area (VFA) were measured at the level of the umbilicus in terms of the CT number by a standardized method. In brief, a region of interest was defined in the subcutaneous fat layer by tracing its contour on each scan, and the attenuation range of fatty tissue was measured in terms of the CT number (in Hounsfield units).

Pathology

The biopsy specimens of liver tissue were stained with hematoxylin-eosin, reticulin, and Masson trichrome stains, and the histopathological findings were scored by